CNIC-00706
CNDC-0011
INDC(CPR)-029/L

COMMUNICATION OF NUCLEAR DATA PROGRESS

No. 8 (1992)

China Nuclear Information Center
Chinese Nuclear Data Center
Atomic Energy Press

CNIC-00706
CNDC-0011
INDC(CPR)-029 / L

COMMUNICATION OF NUCLEAR DATA PROGRESS

No. 8 (1992)

Chinese Nuclear Data Center

China Nuclear Information Centre

Atomic Energy Press

Beijing, Dec., 1992

EDITORIAL NOTE

This is the eighth issue of *Communication of Nuclear Data Progress* in which the achievements in nuclear data field during the last year in China are carried. It includes the measurements of secondary neutron spectra on ^{9}Be, the cross section and angular distribution of $^{40}Ca(n,\alpha)$ reaction, ^{54}V decay data and $^{107}Ag(\alpha,n)$ cross section; the theoretical calculations of neutron induced reaction data ^{56}Fe, ^{238}U and proton induced reaction data on ^{89}Y and ^{241}Am; the charged particle data evaluation of ^{235}U; and some papers about atomic and molecular data and data processing.

We hope that our readers and colleagues will not spare their comments in order to improve the publication.

Please write to Drs. Liu Tingjin and Zhuang Youxiang
Mailing Address : Chinese Nuclear Data Center
China Institute of Atomic Energy
P. O. Box 275 (41), Beijing 102413
People's Republic of China
Telephone : 9357729 or 9357830
Telex : 222373 IAE CN
Facsimile : 86–1–935 7008.

CONTENTS

I EXPERIMENTAL MEASUREMENT

THE MEASUREMENT OF THE BERYLLIUM SECONDARY NEUTRON SPECTRA

Zhang Kun Cao Jianhua Wan Dairong Dai Yunsheng

(INSTITUTE OF NUCLEAR SCIENCE AND TECHNOLOGY OF SICHUAN UNIVERSITY)

ABSTRACT

The beryllium secondary neutron time–of–flight spectra induced by 14.7 MeV neutrons have been measured with an associated particle time of flight spectrometer at the laboratory angles of 15, 25, 35, 45, 60, 75, 90, 105, 120 and 135 degrees. The flight path of secondary neutrons is 254 cm. The bias is 0.9 MeV of the spectrometer and the time resolution is about 1.5 ns. The effective energy ranges is 1.0 MeV to 14.7 MeV for the secondary neutron spectra and the statistical error is 4～10%.

INTRODUCTION

Since beryllium's unique characteristic of emitting two neutrons for each inelastic neutron interaction and often considered as the first structural material of fusion reactors, the neutron data for beryllium is especially important. The neutrons emitted from beryllium can be used to produce tritium, which is one of the major components of the reactor. To calculate the tritium breeding rate in proposed reactor vessel walls requires the detailed knowledge of the energies and angular distributions of the neutrons emitted from beryllium under the bombarding of the energetic neutrons.

Some of the experiments on beryllium were reported for incident neutrons of 5.9, 10.1 and 14.2 MeV[1], and 14.1, 18.0 MeV[2, 3], and so on. In present

work, the angular distributions of the neutron emission spectra from beryllium at incident neutron energy of 14.7 MeV were measured. Now we are going to compare the data with those of the reported experiments and other evaluated data concerning the emission spectra and particle scattering cross sections derived from the energy–angular neutron spectra and double–differential neutron scattering cross sections. In this paper, only the secondary neutron time–of–flight spectra are given.

1 EXPERIMENTAL METHOD

To measure energy–angular continuum neutron spectra, the monoenergetic neutrons are essential. The primary neutron source in present experiment was obtained via the $T(d,n)^4He$ reaction with solid tritium–loaded titanium targets which were cooled by water. The emitted neutrons at angles of 39 degrees and with 14.7 MeV were measured by means of an associated particle time of flight spectrometer.

The neutron detector consists of a 100 mm–diam. × 50 mm–thick ST 451 liquid scintillator directly coupled to an XP–2401 photomultiplier. It was placed in a massive shield which was made up of Li_2CO_3, paraffin, Fe and Pb, and set on a turning table. The neutron–γ discrimination was completed by the CANBERRA, PSD–2610 NIM model based on the zero–crossover technique. The time–of–flight signal of the secondary neutrons was digitized into about 0.28 ns per channel by CANBERRA TIME ANALYZER MODEL 2043 (TAC) and CANBERRA ADC 8075. The time spectra were stored in computer. The bias of the neutron spectrometer is set at 0.9 MeV, the time resolution is 1.5 ns and the effective energy range is from 1.0 MeV to 14.7 MeV for the secondary neutron energy spectra.

The relative efficiency curve of neutron detector was determined by measuring the elastic scattering neutrons from the H(n,n)H reaction with polyethylene sample and C(n,n)C reaction with carbon in the neutron energy ranging from 0.98 MeV to 14.7 MeV.

The scattering samples were machined into the shape of right cylinders, 40 mm–diam. × 20 mm–thick for the beryllium sample, 33.8 mm–diam. × 24.5 mm–thick for the polyethylene and 40 mm–diam. × 35 mm–thick for the carbon, respectively. These samples were placed 10 cm away from the target.

2 DATA ANALYSIS AND RESULTS

To eliminate the count from discrete levels of carbon in the time spectra

from polyethylene for the efficiency calibration, both spectra from carbon and polyethylene samples were measured at each angle, and were normalized according to the elastic scattering of carbon. Fig. 1 presents the time spectra of polyethylene and carbon at 45 laboratory degrees.

For the time spectra acquired with an associated particle time–of–flight spectrometer, the channel counts on right to the elastic peak not correlative each other and are only accidental coincidence. The average count of these channels is named average background for the time spectra. The effective time spectra are obtained via the count of every channel minus the average background.

The secondary neutron time spectrum of beryllium and its background spectrum at 75 degrees are shown in Fig. 2. For the background spectrum, there is no different between the high energy side and the low energy side. Their average values are equal.

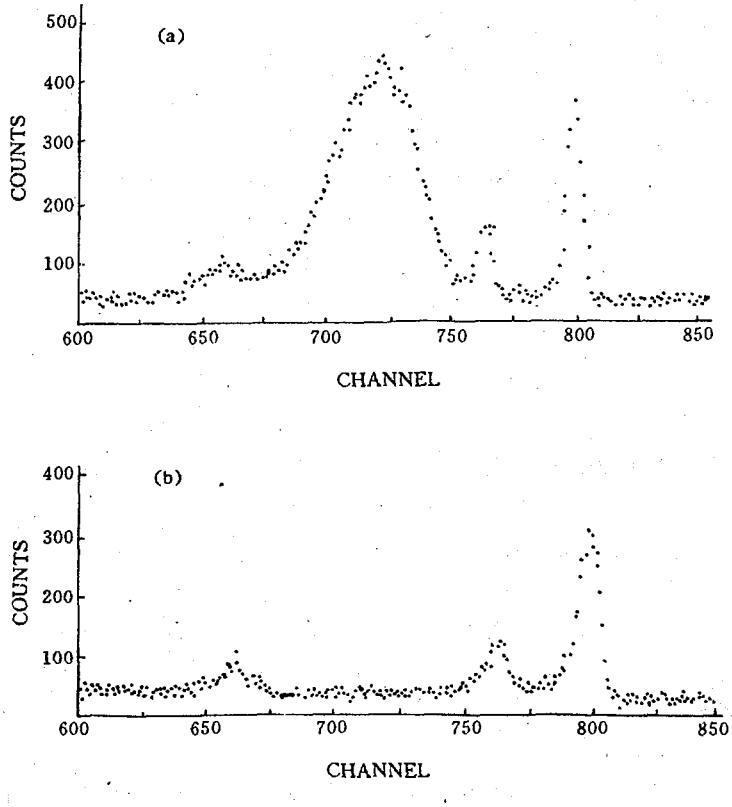

Fig. 1 Emission neutron TOF spectra from polyethylene (a) and carbon (b) at 45 degrees

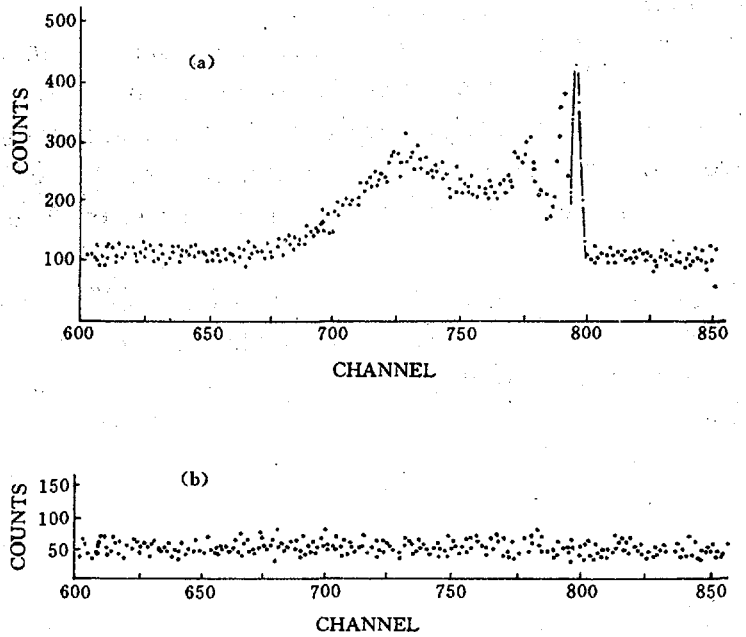

Fig. 2 Emission neutron TOF spectra from beryllium
(a) and its background (b) at 75 degrees

In the nonrelativistic condition, the flight time of neutron is as following[4]:

$$t(\mathrm{ns}) = 72.298L(1 + 0.798 \times 10^{-3}E) / \sqrt{E} \tag{1}$$

here L is the flight path of the secondary neutron with energy E. Therefore, the channel address Ni of the neutron with energy E_i can be determined by the following function for the time spectra :

$$N_i = N_e - 72.298[(1 + 0.798 \times 10^{-3}E_i) / \sqrt{E_i} - (1 + 0.798 \times 10^{-3}E_e) / \sqrt{E_e}]L / W \tag{2}$$

here E_e and N_e are the scattering neutron energy and channel address, respectively; W is the channel width of the time spectrum.

Using this formula, secondary neutron energy spectra can be obtained from the time spectra. In the experiment, these time spectra are given at 10 angles for beryllium, 11 angles for polyethylene, and 8 angles for carbon.

REFERENCES

[1] D. M. Drake et al., Nuclear Science and Engineering, 63, 401(1977)
[2] B. Mamour et al., Nuclear Data for Science and Technology, Mito, 209(1988)
[3] T. Akito et al., Nuclear Data for Science and Technology, Mito, 205(1988)
[4] G. Shen et al., Chinese Journal of Nuclear Physics, 3, 288(1986)

MEASUREMENT OF CROSS SECTION AT 5 MeV AND ANGULAR DISTRIBUTION AT 4 AND 5 MeV FOR REACTION OF $^{40}Ca(n,\alpha)^{37}Ar$

Tang Guoyou Bao Shanglian Qu Decheng
Zhong Wenguang Cao Wentian

(PEKING UNIVERSITY)

Chen Zemin Chen Yingtang Qi Huiquan

(TSINGHUA UNIVERSITY)

Yd. Gledenov Huuhanhuu

(JOINT INSTITUTE FOR NUCLEAR RESEARCH, DUBNA 141980, RUSSIA)

INTRODUCTION

The cross sections and angular distributions of α–particles from neutron induced reactions are important both for applications[1] and nuclear structure research[2]. ^{40}Ca is a double magic nucleus. But the parameters of optical model were not normal[3]. The large difference existed between the data of the cross sections calculated with compound nucleus and pre–equilibrium theory and the experimental measured ones[1, 4, 5] for charge particle emission channel of natu-

ral calcium. Natural calcium is one of structure material of nuclear reactors, and the abundance of ^{40}Ca is 96.94% in nature calcium. Up to now, the existed data of the cross sections and angular distribution for α–particle from the reaction in the energy range from 3 to 7 MeV are scarce and have large discrepancy with each other[1]. Therefore the measurement and calculation of the data are significant.

1 THE SET UP OF THE EXPERIMENT

The experiment was carried out using the mono–energy neutron source of the 4.5 MeV Van de Graff in the Institute of Heavy Ion Physics, Peking University (IHIP, PK), P. R. China[6], which was a Chinese product and just put into running recently.

The experiments were carried out with a gridded ion chamber as the detector of α–particles. Because the high detection efficiency and the good energy and mass resolution, the ion chamber was satisfied for the experiment. And the information of the angular distribution of α–particles could also be driven from the measured data. The chamber was made in Neutron Laboratory of Joint Institute of Nuclear Research (NL, JINR), Dubna, Russia.

The primary result, that was obtained cooperated with Tsinghua University, will be published on Physics Bulletin in 1992.

The detail introduction of the experimental set up were presented as following.

1.1 The Detector of α–Particles

The detector of α–particles was the gridded ion chamber (Fig. 1). The shell of the chamber was made of aluminum. The thickness of the shell was 3 mm. The diameter of the chamber was 37 cm. The electrodes of the chamber was vertical to the bottom plane and were made of tungsten with high purity. The electrodes were structured with thin tungsten plane in rectangular shape at size of 20×20 cm^2. The grids of the chamber were made of golden electroplated tungsten wires of 0.1 mm in diameter and 2 mm in space. The distance of the electrodes between the cathode and the first grid was set up as 3 cm that was enough to stop all the interested α–particle in the active volume[7]. The distance between first grid and second one was 5 cm. The distance between second grid and anode was 2 cm. The high voltage of the electrodes of the chamber were $V_c = 3000$ V, $V_{g1} = -2430$ V, $V_{g2} = -960$ and $V_a = 0$. All these voltage supplies were satisfied to the condition to make that the electron capture in

grids could be negligible[7]. A movable Pu–α source, which was hid in top of the chamber during the accelerator beam time and was inserted in the front of cathode during the energy calibration of the measuring system. The spectrum of the α–particles was shown in Fig. 2a and 2b. The working gas of the chamber was mixed with 95% Ar and 5% CO_2 at pressure of 0.16 bar.

The emission angle of the α–particle was taken using formulate[8]:

$$\cos\theta = \frac{d}{X(E)} \times (1 - R\frac{G_a}{G_c}) \tag{1}$$

where d was the distance of the cathode and first grid (3cm), $X(E)$ was the distance between the start point of α ionization trace and the center of the ionization trace gravity, which was calculated with TRIM90 code. R was the constant that was mainly determined by the amplitude ratio of the anode and cathode signals and little influenced by grid inefficiency (in our case the influence could be negligible), G_a and G_c were the amplitudes of anode and cathode signals.

1.2 The Target Used in the Experiment

The target used in the experiment was a CaF_2 layer in diameter of 5 cm, which was made by evaporation in vacuum on aluminum foil. The thickness of target was 0.86 + 0.03 mg / cm^2, which was determined by the weighting method. The purity of CaF_2 was 99.9%. The contaminator of other α–particles from other isotopes of calcium could be negligible. The background caused by scattering on the chamber structure materials was measured by a dummy sample in turning 180° of the chamber.

1.3 The Electronics and Nuclear Data Acquisition System

The block diagram of the electronics and multiple parameter system are shown in Fig. 3. The charge sensitive preamplifiers were used in the experiment. The main amplifiers were ORTEC 570 with gain 50 and shaping time 2μs. Because the time difference between anode and cathode signals were about a few micro–second, a delay and stretcher ORTEC 542 was needed for making time in coincidence of the signals, in which the random background was reduced.

The data acquisition system was a multiple parameter system that was designed and produced in IHIP recently[9]. The system was based on IBM compat-

ible personal computer. Two data blocks in memory were assigned as data buffer. One of the two buffers used as data acquisition. When the first buffer was full, then the second one started to acquire automatically. Because the data transfer method used in the system was DMA, then CPU could transfer the data from the fulled buffer to permanent exit storage device for further off line analysis without stopping the data acquisition in another buffer. The size of the buffer can be changed by software that depends on the counting rate of the system. The maximum size of the data buffer was 64 k for each. For the number of the parameters, user could make a choise on their own wishes from one to four.

2 THE RESULT AND DISCUSSION

2.1 Angular Distribution

The two dimensional pictures of the anode and cathode signals were shown in Fig. 4a and b for the reaction $^{40}Ca(n,\alpha)^{37}Ar$ at 4 and 5 MeV. The information of angular distribution was deriven from formula (1) and the results were shown in Fig. 5a and 5b. In order to reduce the uncertainty only the events in the solid angle smaller than 75° (the normal line of the target is 0°) were used. The uncertainties involved were the calculation uncertainty of $X(E)$, event statistics and the background subtraction. Up to now the only existed data of angular distribution for reaction $^{40}Ca(n,\alpha)^{37}Ar$ were measured in 1964 by Cavallaro[11] at energy of 3.6 ± 0.25 MeV and 4.0 ± 0.125 MeV. Their result at 4 MeV was also shown in Fig. 5c for comparison. The shape of the angular distribution was quite different from us, and the peak in forward angle was difficult to understand, as our result shown that the angular distribution at 4 MeV was symmetry to 90°. At 5 MeV the data was somewhat forward.

2.2 The Cross Section at 5 MeV

From the measurement the cross section of the reaction was also derived as:

$$\sigma_{n,\alpha} = 234 \pm 23 \text{ mb} \qquad (2)$$

which is consistent with the result measured by C. M. Bartle et al. [10] in 1981 within the uncertainty. The neutron fluency was determined by a calibrated long counter of BF_3 in our case. The uncertainties in present work are from the uncertainty of neutron fluency determination, attenuation of neutrons on win-

dow of ion chamber and electrodes, uncertainty on the determination of target thickness and the uncertainty from background subtraction.

ACKNOWLEDGEMENT

The present work was partly financially supported by China National Nuclear Company. Authors wish to thank Dr. Zhang Yingxia, Lu Jianqing, Wang Jianyong and Xu Pinfang for their help in accelerator operation.

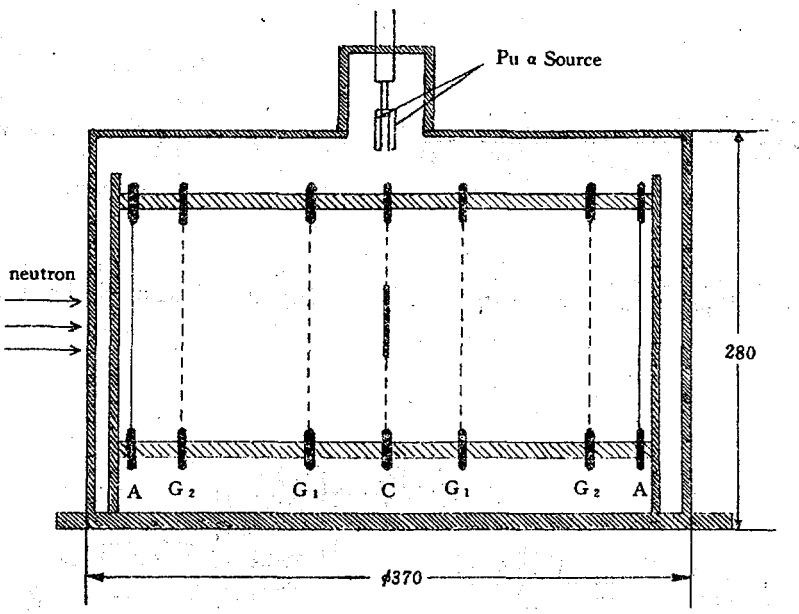

Fig. 1 The diagram of the double gridded ion chamber

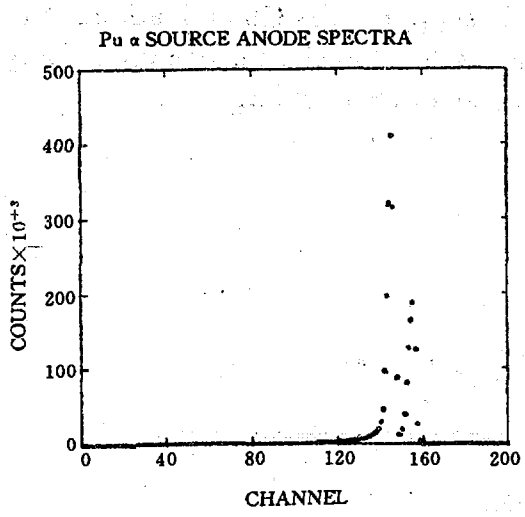

Fig. 2a The anode α Spectrum

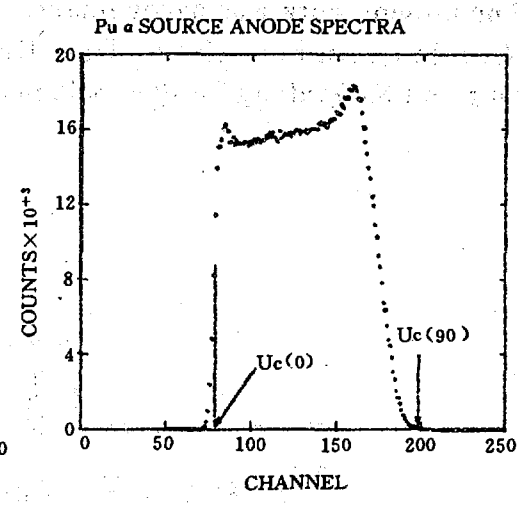

Fig. 2b The cathod α spectrum

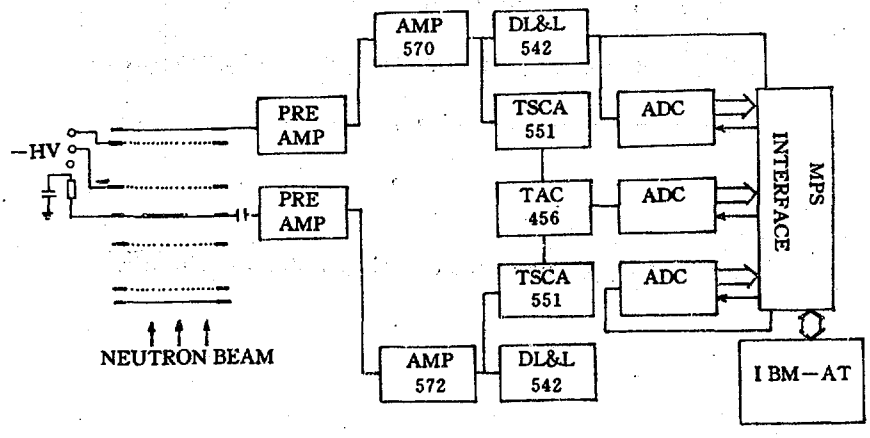

Fig. 3 Block diagram of data acquisition system

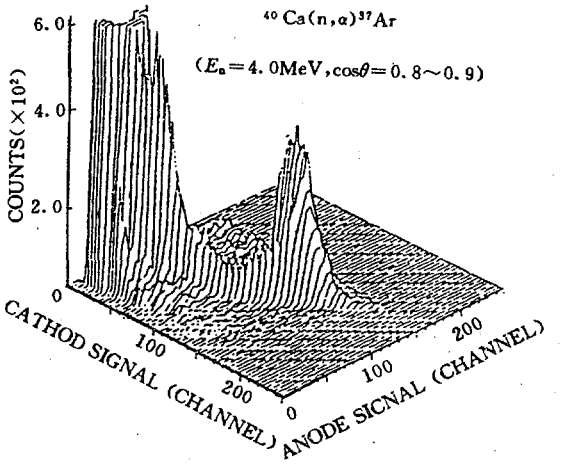

Fig. 4a The two dimensional α spectrum

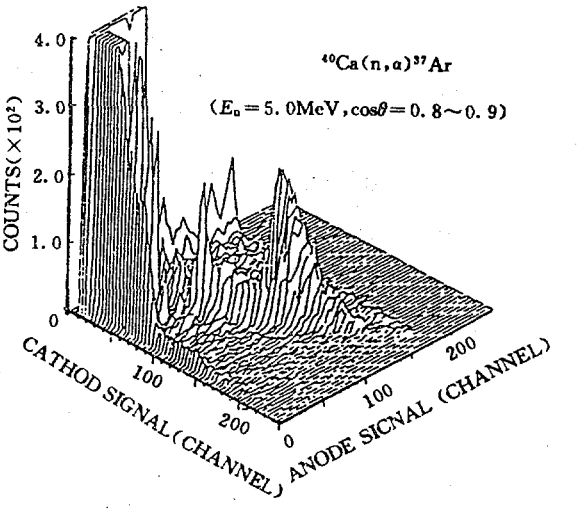

Fig. 4b The two dimensional α spectrum

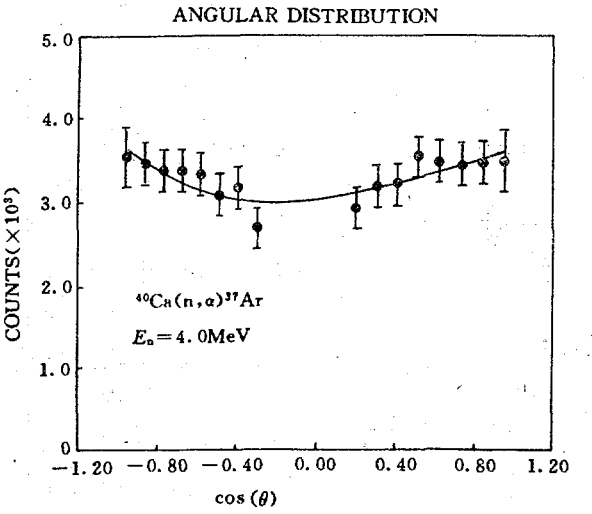

Fig. 5a The α angular distribution (4 MeV)

DECAY OF ^{54}V

Chen Xueshi Zhu Jiabi Xie Kuanzhong

(SHANGHAI INSTITUTE OF NUCLEAR
RESEARCH, ACADEMIA SINICA)

When evaluating the data of ^{54}V decay, we found that the available data are rather discrepant[1, 2]. It is necessary to check the data with our own experiments. The radionuclide ^{54}V was produced by the fast neutron (n,p) reaction on a 50 mg sample of 90% isotopically enriched ^{54}Cr. The 14.6 MeV neutrons, the yield of which was $1.5\sim 2.0\times 10^9$ neutrons / s, were generated through the T(d,n) reaction using the 200 kV Cockcroft–Walton accelerator. A " rabbit " system was used to transport the sample between the places of irradiation and detection. The " rabbit " system and the detection system were controlled with a programmable Multichannel Analyzer of ND66B, as shown in Fig. 1. The measurement procedure is as following : bombarding 1 to 4 half lives; cooling 1 / 2 to 1 half life; then measuring 5 sequent MCA spectra, each one for 1 half life. A spectrum without sample was determined as the background in accelerator working condition. For getting the sufficient statistics, 150 to 200 cycles were needed to accumulate the data. The detecting system was so stable that shifts of the spectra were $<\pm$ 1 ch. during the whole experiment time of 30 to 40 h.

A coaxial Ge(Li) detector with a resolution of 2.1 keV FWHM for ^{60}Co 1332 keV γ–ray and a NaI(Tl) ($\varphi 7.6\times 7.6$ cm) detector were used to study the radiation from the de–excitation of ^{54}Cr following the β–decay of ^{54}V. The radiosources of ^{56}Co (half life 77.3 days) produced through $^{56}Fe(p,n)$ reaction using the cyclotron at our institute, ^{60}Co, ^{133}Ba, ^{40}K and ^{208}Tl were used to make the energy calibration for γ–rays in spectra of Ge(Li) detector from 0.2 to 4.0 MeV.

The uncertainties of energy : < 2 keV, the uncertanties of intensity : $\pm$ (1 $\sim$2%). According to energies, half lives, intensities and other knowledges we can determine the sources where the γ–rays come from. The results are collected in Table 1. The average half life of ^{54}V is 46.4 ± 0.6 sec. and 19 γ–rays belonging to ^{54}Cr de–excitation were measured. It turns out that the Nathan's[2] are close to our's.

The aim of using NaI(Tl) detector was to search the new γ–rays with high

energies and low intensities. From the NaI(Tl) γ–spectra we clearly saw two new γ–rays with energies of about 4.56 and 5.0 MeV. Since the released energy from β–decay of ^{54}V is 7.0 MeV, these two high γ–rays could belong to the de–excitation of high energy states of ^{54}Cr. Of course which states are they? That should be confirmed with further coincidence experiments.

The authors would like to thank Prof. Xue Liudong for his help in setting up the control system and to Dr. Zhang Bufa and Mr. Lu Rong and Ye Bonian for operation of the accelerator.

Table 1 γ–ray energies intensities and half lives from the decay of ^{54}V

E_γ (keV)	I_γ (%)	$T_{1/2}$ (s)
563.72	4.8	
834.54	100	46.8
987.93	76.5	46.7
1334.46		
1398.84	5.9	
1461.32		
1782.50		
1832.42	3.9	
1963.05	9.5	
1974.41	4.1	
2239.44	4.2	
2260.26	52.4	45.6
2326.52	0.7	
2394.67	3.0	
2602.89	1.1	
2621.81		
2629.00		
2964.40	2.9	
3382.65	3.3	
4650		
~5000		

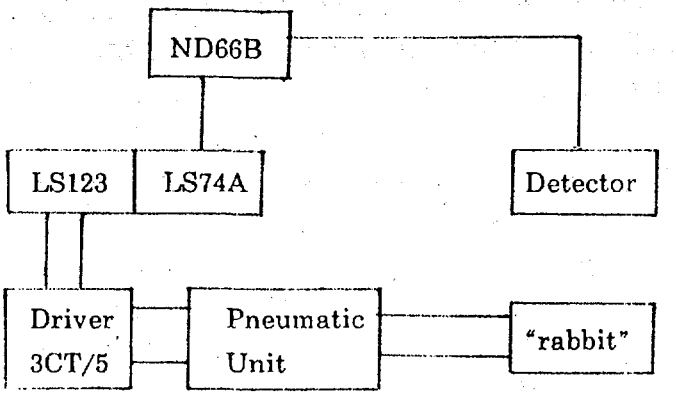

Fig. 1 ND66B controlled system

REFERENCES

[1] T. E. Ward et al., Nuclear Physics, A148, 225(1970)

[2] A. M. Nathan et al., Physics Review, C16, 1566(1977)

MEASUREMENT OF EXCITATION FUNCTIONS FOR REACTIONS $^{107}Ag(\alpha,n)^{110m}In$, $^{107}Ag(\alpha,2n)^{109}In$ AND $^{109}Ag(\alpha,2n)^{111}In$

Peng Xiufeng Liu Mantian He Fuqing Long Xianguan

(INSTITUTE OF NUCLEAR SCIENCE AND TECHNOLOGY, SICHUAN UNIVERSITY)

Nuclides ^{110m}In, ^{109}In and ^{111}In are useful radioisotopes, especially ^{111}In, which has suitable short-life (2.83d) for being produced by accelerator, is one of the photon emitters most widely used for radiomedical application, mainly for antibody and cell labelling.

The excitation functions of reactions $^{107}Ag(\alpha,n)^{110m}In$, $^{107}Ag(\alpha,2n)^{109}In$, and $^{109}Ag(\alpha,2n)^{111}In$ have been determined. The irradiation of natural silver foil (purity better than 99.99%) with 26.8 MeV alpha beam was carried out at the 1.2 m cyclotron in Institute of Nuclear Science and Technology, Sichuan University, Chengdu. The yield of the radioactive products was measured using a well calibrated HPGe detector in a low background chamber, a computer system was adopted to acquire and analysis data.

The present results are given in table 1.

Table 1 Experimental cross section values in millibarn

E_α (MeV)	$^{107}Ag(\alpha,n)^{110m}In$	$^{109}Ag(\alpha,2n)^{111}In$	$^{107}Ag(\alpha,2n)^{109}In$
10.4	0.15		
13.1	12.0	0.6	
15.5	101.8	73.8	
17.6	207.0	339.3	117.0
19.6	214.7	598.1	354.5
21.4	138.4	364.4	570.0
23.2	83.2	898.0	724.6
24.8	50.2	966.0	807.3
26.3	44.7	1052.9	849.3

II THEORETICAL CALCULATION

CALCULATION OF NEUTRON INDUCED REACTION ON ^{56}Fe IN ENERGY REGION 5~50 MeV WITH PROGRAM CMUP2

Shen Qingbiao

(CHINESE NUCLEAR DATA CENTER, IAE)

Cai Chonghai

(DEPARTMENT OF PHYSICS, NANKAI UNIVERSITY, TIANJIN)

ABSTRACT

A set of neutron optical potential parameters for ^{56}Fe in energies of 5~50 MeV is obtained based on the available experimental data. Various calculated nuclear data are in good agreement with the experimental data. Some conclusions on reaction mechanism were obtained.

INTRODUCTION

The studies of nuclear reaction in $E < 50$ MeV energy region are significant for nuclear data applications, such as the macroscopic test to the microscopic neutron data for fusion reactor, the medical radioisotope production and the studies of radioactive nuclear beams. When the projectile energy approaches to 50 MeV, there exist tens of multi-particle emission channels and the reaction process becomes very complicated. The direct reaction and the preequilibrium emission process are more important. Taking neutron induced reactions on ^{56}Fe in energy region 5~50 MeV as example, the calculations and analyses

of the nuclear reactions were carried out with the program CMUP2 recently.

1 THEORIES AND PARAMETERS

The optical model, evaporation model, and preequilibrium emission theory exciton model were used in our calculations. The (n,n′) direct inelastic scattering contributions were obtained by the collective excitation distorted–wave Born approximation. The compound–nucleus elastic scattering contributions were calculated by Hauser–Feshbach theory.

The multi–particle and hole state densities considered the Pauli exclusion principle in the exciton model were used[1~4].

For composite particle emission, the pick–up mechanism of cluster formation[5~7] was accepted. Because of higher incident energies, the preequilibrium mechanism and the pick–up mechanism of composite particle formation were included in the first, second, and third particle emission processes.

Firstly, a program APNOM[8] was made, by which the optimum neutron optical potential parameters can be searched automatically by fitting experimental total, nonelastic cross sections and elastic scattering angular distributions. Secondly, based on optical model, evaporation model, and preequilibrium emission theory, a program CMUP2[9] was developed, by which neutron or charged particle induced reactions for medium–heavy nuclei with incident energies up to 50 MeV can be calculated. The Gilbert–Cameron level density formula[10] was applied.

Based on various experimental data of ^{56}Fe from EXFOR and BNL–325 [11], a set of optimum neutron optical potential parameters was obtained as follows :

$$V = 54.3759 - 0.48634E + 0.003575E^2 - 24.0(N-Z)/A \quad (1)$$

$$W_S = 11.5977 - 0.26697E - 12.0(N-Z)/A$$

or zero, whichever is greater (2)

$$W_V = -0.89256 + 0.15548E - 0.00007E^2$$

or zero, whichever is greater (3)

$$U_{so} = 6.2 \quad (4)$$

$$r_r = 1.1939, \quad r_S = 1.3659, \quad r_V = 1.4828, \quad r_{SO} = 1.1939 \quad (5)$$

$$a_r = 0.62462, \quad a_S = 0.48624, \quad a_V = 0.36001, \quad a_{SO} = 0.62462 \quad (6)$$

With this set of parameters and adjusting some charged particle optical poten-

tial and level density parameters as well as taking the exciton model constant $K = 300$ MeV^3, the calculated results by the program CMUP2 are in good agreement with the experimental data.

2 CALCULATED RESULTS AND ANALYSES

Fig. 1 shows the comparison of neutron total cross sections between the theoretical values and the evaluated values taken from ENDF / B–6 for energies below 20 MeV and an eye guide curve for 20~ 50 MeV[11]. The calculated results are in good agreement with the experimental data. Fig. 2 shows the calculated neutron nonelastic cross sections. They are in reasonable agreement with the experimental data. Fig. 3 shows that the calculated elastic scattering cross sections agree with the experimental data pretty well. The comparisons of calculated neutron elastic scattering angular distributions of ^{56}Fe from 5.0 MeV to 26.0 MeV with the experimental data are given in Fig. 4. They are in excellent agreement with each other. Based on this fitting situation shown in Figs. 1~4, a set of neutron optical potential parameters were determined.

In order to calculate the direct inelastic scattering cross sections, one must know the deformed parameter β for every discrete level which are listed in Table 1 obtained by fitting the experimental discrete level inelastic scattering angular distributions with DWBA calculations[12]. Table 1 also gives the neutron direct inelastic scattering cross sections $\sigma^{(d)}_{n,n'}$ calculated with the program DWUCK4[13] at 14.1 MeV. One can clearly see that the calculated direct inelastic cross sections for 2^+ state at energy 0.85 MeV and 3^- state at energy 4.51 MeV are larger than other states evidently, since their deformed parameters are larger than others. In comparison of the direct inelastic cross sections of 2^+ state and 4^+ state, in general, the contribution of 4^+ state is much less than that of 2^+ state. The calculated total direct inelastic cross section at 14.1 MeV is 126.6 mb, whereas the cross section contributed by statistical process is 589.2 mb. The former occupies the percent of 18%.

The calculated emitted particle energy spectra by program CMUP2 are continuous because the continuous energy levels are only included in evaporation model and preequilibrium emission theory. Considered the limited experimental resolving power, the calculated discrete energy level cross sections are generally treated with the broadening method in order to compare them with the experimental data. The Gaussian distribution is chosen :

$$p(x)=\frac{1}{\sqrt{2\pi}\,\Gamma}\exp[-\frac{(x-\mu)^2}{2\Gamma^2}] \tag{7}$$

where μ is the position of the discrete level in MeV. Takahashi et al.[14] and Baba et al.[15] measured the emitted neutron energy spectra of ^{56}Fe for (n,xn) reaction at energy 14.1 MeV. Because the measured data include the elastic scattering contributions, we also broadened the calculated neutron elastic scattering cross sections and added them on the inelastic energy spectra. Through many tests, Γ= 0.35 MeV was chosen. Fig. 5 shows the comparison of the calculated and experimental emitted neutron energy spectra for (n,xn) reaction at energy 14.1 MeV in mass center system. The calculated results basically agree with the experimental data. For the elastic scattering peak, the calculated results agree with Takahashi et al. measured data pretty well. There is a small peak at about 9 MeV for both the theoretical curve and measured data. It corresponds to the 3^- state at energy 4.51 MeV. The other discrete energy levels can not be clearly distinguished in Fig. 5 because their cross sections are broadened and covered by elastic scattering peak.

Table 1 The deformed parameter β and the calculated direct inelastic cross sections at 14.1 MeV

I^π	E (MeV)	β	$\sigma_{n,n'}^{(d)}$ (mb)
2^+	0.85	0.252	79.89
4^+	2.09	0.079	0.010
2^+	2.66	0.062	4.19
2^+	2.96	0.040	1.69
4^+	3.12	0.110	0.035
2^+	3.37	0.095	9.42
2^+	3.60	0.063	4.02
2^+	3.83	0.047	2.18
4^+	4.12	0.100	0.022
2^+	4.40	0.059	3.25
3^-	4.51	0.200	21.89

In Fig. 6, the calculated inelastic scattering cross sections and their direct reaction contributions are given. The calculated results are in reasonable agreement with the experimental data. One can clearly see that when the

neutron energy is larger than 30 MeV the main contribution to the inelastic cross section comes from the direct reaction.

Fig. 7 gives the comparison of calculated and experimental (n,2n) cross sections of ^{56}Fe. The agreement between them is not satisfied. The main reason is that we did not consider the discrete level in (n,2n) cross section calculations.

Fig. 8 shows that the calculated (n,p) cross sections are in good agreement with the experimental data. Therefore, the calculated (n,p) cross sections in the 20~50 MeV region, for which there exist nearly no experimental data, are confident.

Fig. 9 shows that the calculated (n,α) cross sections roughly agree with the experimental data. Fig. 10 and 11 show that the calculated (n,d) and (n,t) cross section curves pass through the existent one or two experimental error bars, respectively. Fig. 12 and 13 show that the calculated (n,p–em) and (n,α–em) cross sections basically agree with the experimental data.

Fig. 14 illustrates (n,tot), (n,non), (n,el), (n,in), (n,γ) cross sections and 6 kinds of one particle emission cross sections. Figs. 15, 16 and 17 illustrate calculated various two particle, three particle and four particle emission cross sections, respectively. It is clear that the multi particle emission processes become very important in 20~50 MeV region. Fig. 18 shows calculated n, p, d, t, ^{3}He, and α emission cross sections. Here the emission cross section means the sum of all the cross sections emitting the same particle. One can clearly see that the 5 kinds of charged particle emission cross sections are comparable and that t–em, d–em cross sections are larger than the others in the 25~40 MeV region. Fig. 19 illustrates calculated neutron induced yield cross sections below 40 MeV. Many isotopes of the elements Fe, Mn, Cr, V, Ti, and Sc can be produced in the reaction n+^{56}Fe. It is clear that the higher the neutron energy, the larger the number of yield nuclei.

The percents of the equilibrium and preequilibrium emission cross sections in (n,n′), (n,p), (n,α), and (n,d) single particle emission processes are given in table 2. One can clearly see that when $E_n < 10$ MeV the main contribution to emission cross section comes from the equilibrium emission process. When $E_n = 20$ MeV, more than 90% of contribution comes from the preequilibrium emission process. If $E_n > 25$ MeV, whole contribution is almost obtained from the preequilibrium emission process.

Table 2 Percents of the equilibrium and preequilibrium emission cross sections in single particle emission processes

E_n	(n,n′)		(n,p)		(n,α)		(n,d)	
(MeV)	Eq (%)	Pre(%)	Eq (%)	Pre(%)	Eq (%)	Pre(%)	Eq (%)	Pre(%)
5	97.0	3.0	99.2	0.8	99.97	0.03		
10	76.3	23.7	85.8	14.2	74.4	25.6	100.0	0.0
15	27.3	72.7	52.2	47.8	21.6	78.4	10.6	89.4
20	2.1	97.9	6.7	93.3	2.2	97.8	1.7	98.3
25	0.16	99.84	0.57	99.43	0.16	99.84	0.21	99.79
30	0.03	99.97	0.16	99.84	0.02	99.98	0.01	99.99
35	0.01	99.99	0.10	99.89	0.01	99.99	0.0	100.0
40	0.0	100.0	0.08	99.92	0.0	100.0	0.0	100.0
45	0.0	100.0	0.07	99.93	0.0	100.0	0.0	100.0
50	0.0	100.0	0.05	99.95	0.0	100.0	0.0	100.0

The percents of emission cross sections obtained by three kinds of emission mechanism in two-particle emission processes (n,2n), (n,np), (n,pn), (n,nα), and (n,αn) are given in table 3. The three kinds of emission mechanism are: the two particles all come from the equilibrium emission (Eq); the first particle comes from the preequilibrium emission and the second particle from the equilibrium emission (Pre(1)+Eq(2)); and the two particles are all emitted in the preequilibrium processes (Pre). One can clearly see that when $E_n = 20$ MeV the maximum contribution of the preequilibrium emission of the second particle is 3.5% . As we know for two-particle emission processes only the first particle is emitted by the preequilibrium process, the second particle can also be emitted by the preequilibrium process. Generally speaking, the energy of the first particle, which is emitted by the preequilibrium process, is higher and the residual excitation energy in nucleus is lower, then the probability of the preequilibrium emission of the second particle is rather little. Therefore, above results are reasonable and show that one can neglect the contribution of the preequilibrium emission process of the second particle as the incident energy is less than 20 MeV. One can also see that when $E_n = 50$ MeV the contributions of the preequilibrium emission process of the second particle are 42.5%~88.2%. It means that the preequilibrium emission of the second particle must be taken into account as the incident energy is in 20~50 MeV. Through similar analyses for the calculated results in table 3, one can conclude that the contribution of the preequilibrium emission process of the third particle can be neglected when $E_n < 50$ MeV.

Table 3 The percents of emission cross sections contributed by three kinds of emission mechanism in two particle emission processes

E_n (MeV)	(n,2n) Eq (%)	(n,2n) Pre(1)+Eq(2) (%)	(n,2n) Pre (%)	(n,np) Eq (%)	(n,np) Pre(1)+Eq(2) (%)	(n,np) Pre (%)
12	87.8	12.2	0.0	87.3	12.7	0.0
15	70.08	22.88	0.15	77.08	22.88	0.04
20	38.1	58.4	3.5	48.7	48.9	2.4
25	14.0	75.9	10.1	23.7	66.8	9.5
30	8.1	74.2	17.7	11.4	68.6	20.0
35	0.17	69.40	30.43	0.88	61.05	38.07
40	0.02	62.22	37.76	0.08	51.48	48.44
45	0.0	57.3	42.7	0.0	41.7	58.3
50	0.0	51.5	48.5	0.0	38.9	61.1

E_n (MeV)	(n,pn) Eq (%)	(n,pn) Pre(1)+Eq(2) (%)	(n,pn) Pre (%)	(n,nα) Eq (%)	(n,nα) Pre(1)+Eq(2) (%)	(n,nα) Pre (%)
12	96.4	3.6	0.0	86.2	13.8	0.0
15	87.71	12.28	0.01	77.8	22.2	0.0
20	63.4	35.3	1.3	51.5	45.2	3.3
25	41.7	51.9	6.4	20.7	56.0	23.3
30	25.6	61.5	12.9	6.8	42.8	50.4
35	14.8	64.2	21.0	0.85	30.53	68.62
40	8.3	63.6	28.1	0.08	19.14	80.78
45	4.6	59.0	36.4	0.01	13.89	86.10
50	2.6	54.9	42.5	0.0	11.8	88.2

E_n (MeV)	Eq (%)	(n,αn) Pre(1) +Eq(2) (%)	Pre (%)
12	87.7	12.3	0.0
15	60.8	39.2	0.0
20	20.9	78.2	0.9
25	7.9	85.4	6.7
30	3.2	80.5	16.3
35	1.3	71.8	26.9
40	0.5	64.0	35.5
45	0.2	53.6	46.2
50	0.1	47.8	52.1

3 CONCLUSIONS

Based on the available experimental data, a set of neutron optical potential parameters for ^{56}Fe in energies of 5~ 50 MeV was obtained. Then adjusting some charged particle optical potential and level density parameters as well as taking the exciton model constant $K= 300$ MeV^3, various calculated nuclear data are in good agreement with the experimental data. Therefore, the various predicted cross sections, yields, angular distributions, and emitted particle energy spectra are reliable to some extent.

Through above analyses for the calculated results, one can obtain the following conclusions: 1. When $E_n > 30$ MeV, the main contribution to (n,n′) cross section comes from the discrete level direct reaction. 2. For single particle emission cross section, the main contribution comes from the equilibrium process when $E_n < 10$ MeV, whereas more than 90% of contribution comes from the preequilibrium process when $E_n = 20$ MeV and whole contribution almost comes from the preequilibrium process when $E_n > 25$ MeV. 3. The contribution of the preequilibrium process to the second particle emission can be neglected when $E_n < 20$ MeV and the contribution of the preequilibrium process to the third particle emission can be neglected when $E_n < 50$ MeV.

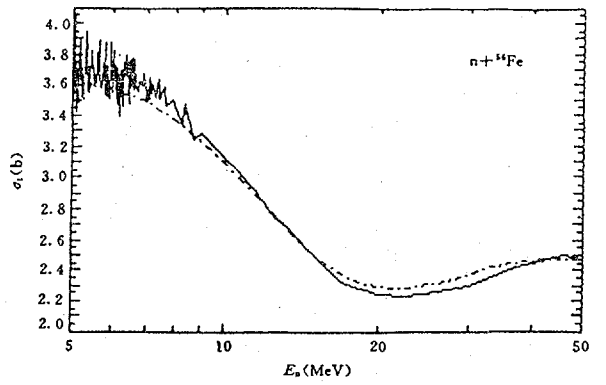

Fig. 1 Comparison of neutron total cross section

—•—• calculated; ——— evaluated.

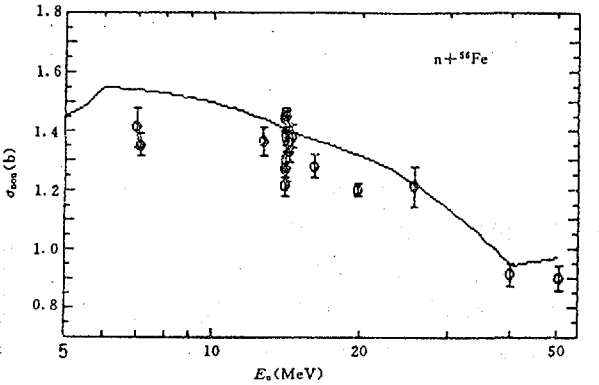

Fig. 2 Comparison of the calculated neutron nonelastic cross sections with the experimental data

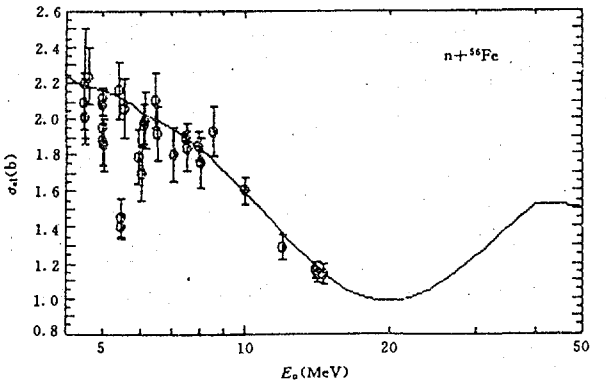

Fig. 3 The same as Fig. 2 except for elastic scattering cross sections

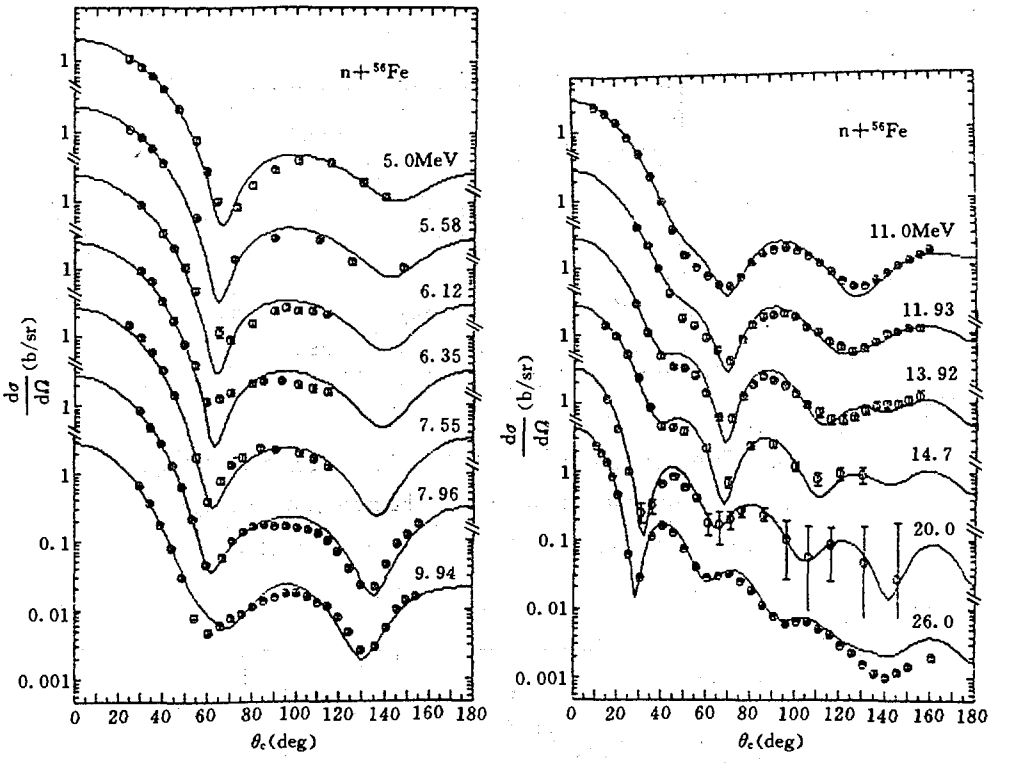

Fig. 4 Comparison of calculated neutron elastic scattering angular distributions with the experimental data

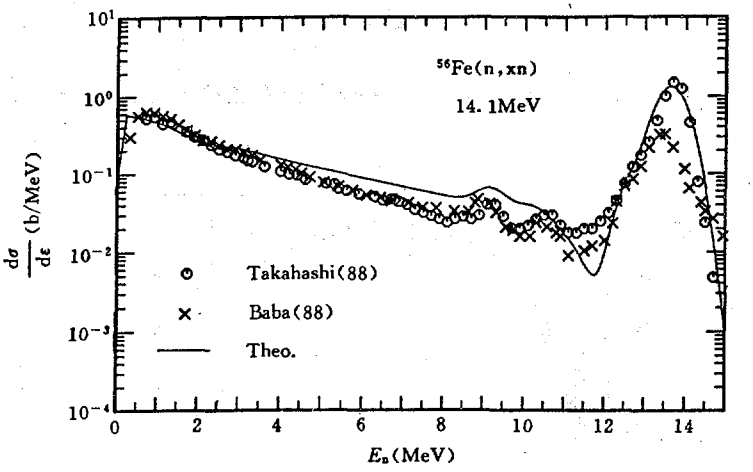

Fig. 5 Comparison of the calculated and experimental emitted neutron energy spectra

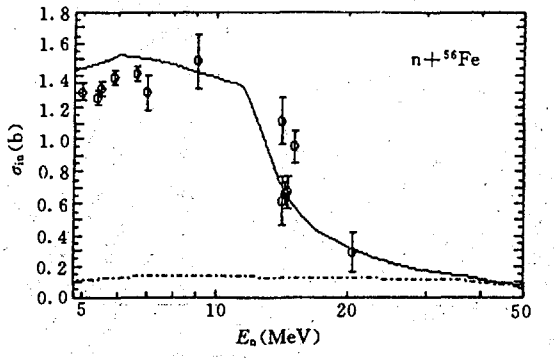

Fig. 6 Comparison of the calculated neutron inelastic scattering cross sections with the experimental data

——— calculated CS; —·—· direct reaction.

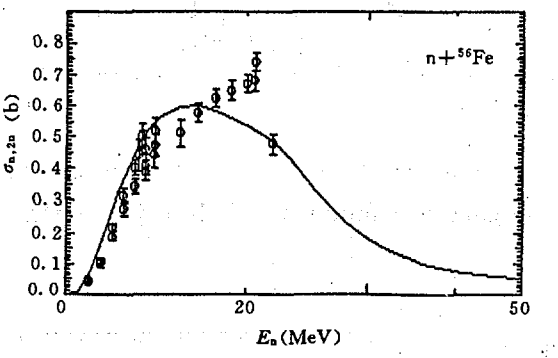

Fig. 7 The same as Fig. 2 except for (n,2n) cross sections

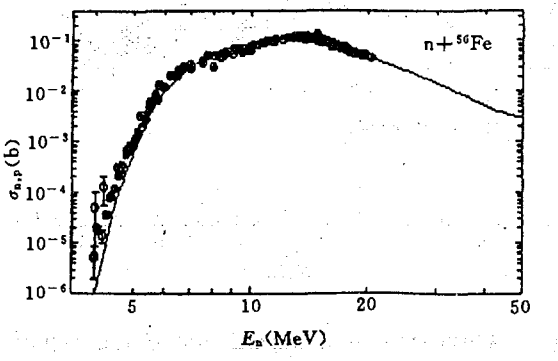

Fig. 8 The same as Fig. 2 except for (n,p) cross sections

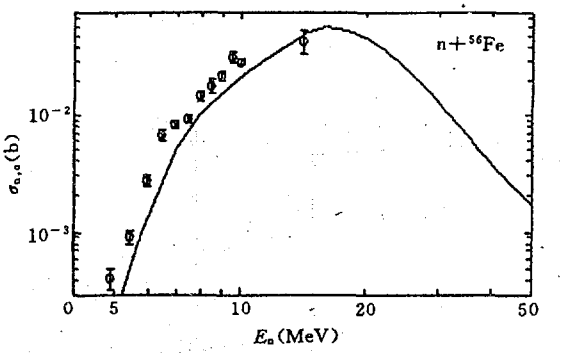

Fig. 9 The same as Fig. 2 except for (n,α) cross sections

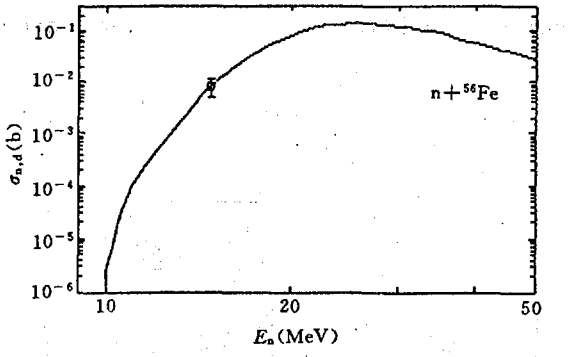

Fig. 10 The same as Fig. 2 except for (n,d) cross sections

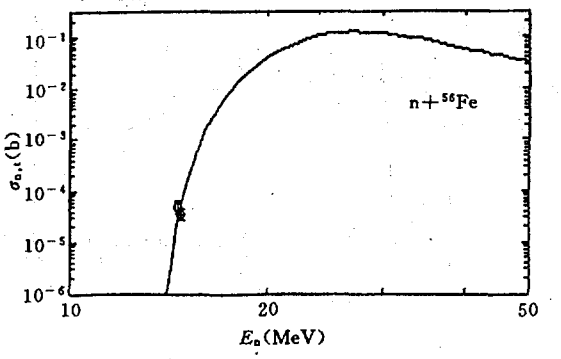

Fig. 11 The same as Fig. 2 except for (n,t) cross sections

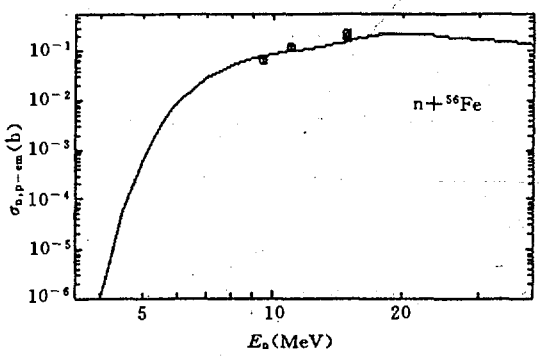

Fig. 12 The same as Fig. 2 except for (n,p–em) cross sections

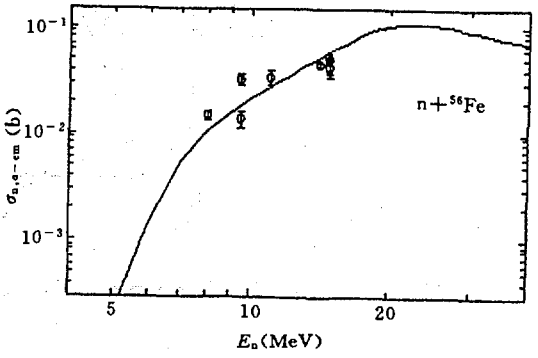

Fig. 13 The same as Fig. 2 except for (n,α–em) cross sections

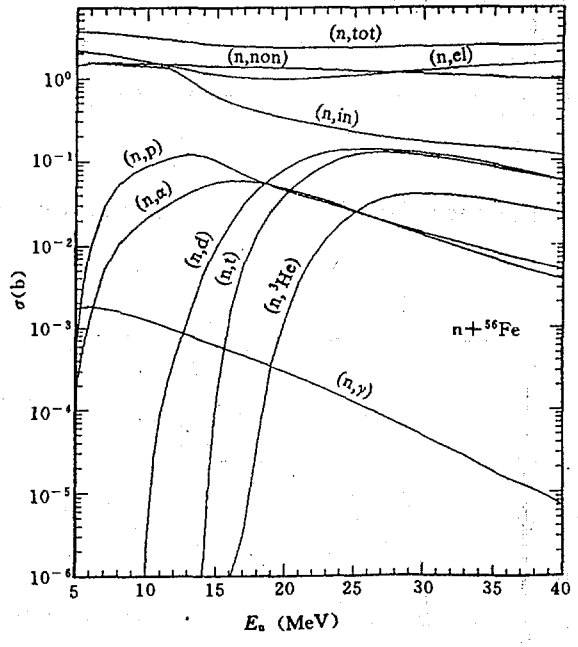

Fig. 14 The calculated (n,tot), (n,non), (n,el), (n,in), (n,γ) and one–particle emission cross sections

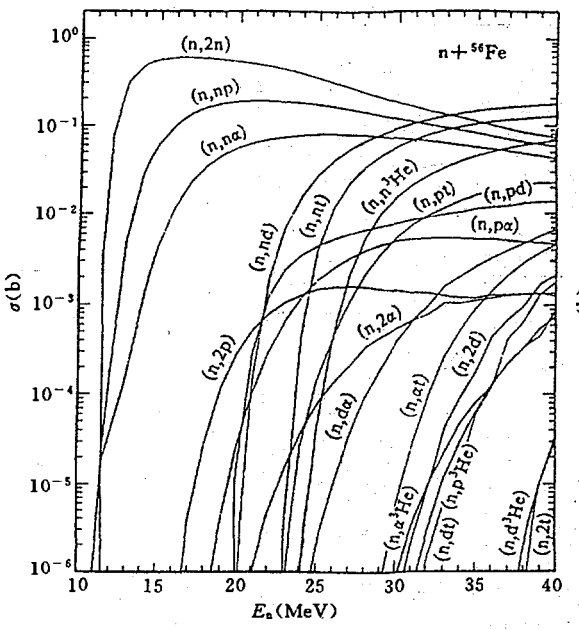

Fig. 15 The calculated two-particle emission cross scctions

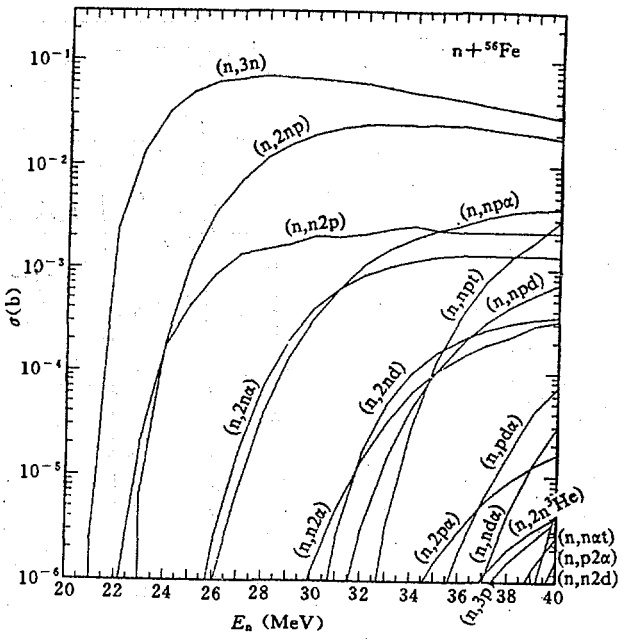

Fig. 16 The same as Fig. 15 except for three-particle emission

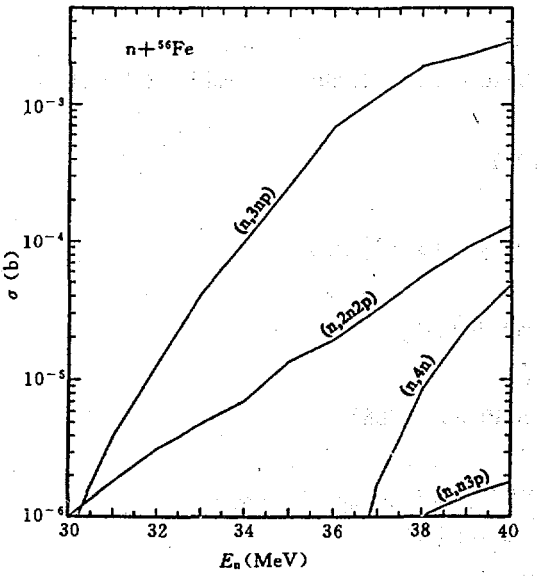

Fig. 17 The same as Fig. 15 except for four-particle emission

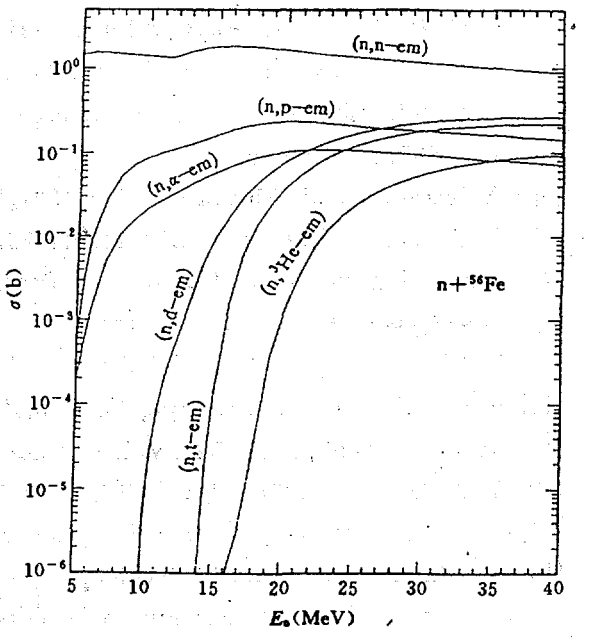

Fig. 18 The calculated emission cross sections for 6 particles

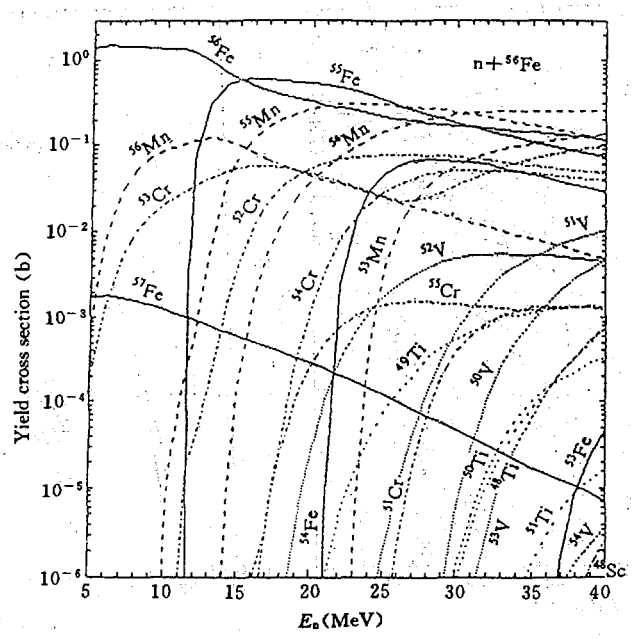

Fig. 19 The calculated yield cross sections in reaction

REFERENCES

[1] M. Bohning, Nucl. Phys., A152, 529(1970)

[2] F. C. Williams, Nucl. Phys., A166, 231(1971)

[3] C. Kalbach, BNL–NCS–51694, p. 113(1983)

[4] Zhang Jingshang et al., High Energy Physics and Nuclear Physics (China), 13, 822(1989) (in Chinese)

[5] A. Iwamoto et al., Phys. Rev., C26, 1821(1982)

[6] K. Sato et al., Phys. Rev., C28, 1527(1983)

[7] Zhang Jingshang et al., Commun. in Theor. Phys., 10, 33(1988)

[8] Shen Qingbiao et al., (unpublished)

[9] Cai Chonghai et al., Nucl. Sci. Eng., (to be published)

[10] A. Gilbert et al., Can. J. Phys., 43, 1446(1965)

[11] V. Mclane et al., BNL–325, Vol. 2, Academic Press, (1988)

[12] S. Mellema et al., Phys. Rev., C33, 481(1986)

[13] P. D. Kunz, "Distorted Wavé Code DWUCK4", University of Colorado

[14] A. Takahashi et al., JAERI–M 88–065, p. 279(1988),
A. Takahashi, private communication (1990)

[15] M. Baba et al., Proc. Conf. on Nuclear Data for Science & Technology, May 30~June 3, Mito, p. 291(1988)

COMPARISON OF DIRECT INELASTIC SCATTERING BETWEEN COUPLED-CHANNEL THEORY AND DWBA METHOD CALCULATIONS FOR ^{56}Fe AND ^{238}U

Shen Qingbiao

(CHINESE NUCLEAR DATA CENTER, IAE)

Liu Dunhuan

(DEPART. OF PHYS., WUHAN UNIVERSITY, WUHAN)

Wu Shunguang Sun Xiuquan

(DEPART. OF PHYS., NORTHWEST UNIVERSITY, XIAN)

ABSTRACT

The direct inelastic scattering cross sections and angular distributions of ^{56}Fe and ^{238}U at incident neutron energies 14.0 and 20.0 MeV were calculated by coupled-channel theory and DWBA method. The calculated results show: 1. For those nuclei, such as ^{56}Fe, coupling between the elastic and inelastic channels is weak, the DWBA method is a reasonable approximation. 2. For large deformation nuclei, such as ^{238}U, the DWBA method is not suitable and the coupled-channel theory needs to be used for calculating the direct inelastic scattering process. 3. The difference of the calculated results by two methods becomes little as incident neutron energy increases.

INTRODUCTION

The direct inelastic scattering is an important process for nuclear data calculation. In most cases, the main contribution to direct inelastic scattering comes from the collective excitation of target nucleus, except for a few filled

shell nuclei. There are two main approaches to calculate the direct inelastic scattering, which are the coupled–channel optical model (CCOM) theory[1] and the distorted–wave Born approximation (DWBA) method[2,3]. The coupled–channel theory of inelastic scattering provides, in principle, an exact way of calculating the cross sections of inelastic reactions. The numerical solution of the coupled equations, even in their truncated form, is however a very laborious process, and in many cases it is sufficiently accurate to use an expression for the scattering matrix element that is exact in the limit of weak coupling between the elastic and inelastic channels.

In this paper, taking the targets ^{56}Fe and ^{238}U and incident neutron energies 14.0 and 20.0 MeV as examples, the calculated direct inelastic scattering cross sections and angular distributions by CCOM and DWBA were compared. Then, one can analyse quantitatively the degree of the approximation of the DWBA method.

1 THEORY AND FORMULA

For nonspherical nuclei, the Hamiltonian of the whole system is as follows:

$$H = -\frac{\hbar^2}{2\mu}\nabla^2 + H_t + V(r,\theta,\varphi) \tag{1}$$

The first term in Eq. (1) is the kinetic energy and H_t is the Hamiltonian for the internal motion of the target nucleus. The nonspherical optical potential $V(r,\theta,\varphi)$ can be divided into two parts:

$$V(r,\theta,\varphi) = V_{\text{diag}}(r) + V_{\text{coupl}}(r,\theta,\varphi) \tag{2}$$

Owing to the presence of V_{coupl}, the radial equations are a group of coupled equations:

$$\left[\frac{\hbar^2}{2\mu}\frac{d^2}{dr^2} - \frac{\hbar^2}{2\mu}\frac{l(l+1)}{r^2} - V_{\text{diag}}(r) + E_n\right] u^{JM}_{nlj}(r) = \sum_{n'l'j'} V^{JM}_{nlj,\,n'l'j'}(r)\,u^{JM}_{n'l'j'} \tag{3}$$

where

$$V^{JM}_{nlj,\,n'l'j'} = \langle (y_{ljm_j} \otimes \Phi_{I_n M_n})_{JM} | V_{\text{coupl}}(r,\theta,\varphi) | (y_{l'j'm'_j} \otimes \Phi_{I'_n M'_n})_{JM} \rangle \tag{4}$$

One can prove that above equations are M independent.

Let channel labels $\alpha = (nlj)$ and $\alpha' = (n'l'j')$ and substitute $LV_{\text{diag}}(r)$ by $V_\alpha(r)$. Then the Eq. (3) can be written as

$$\left[\frac{d^2}{dr^2} - \frac{l(l+1)}{r^2} + K_\alpha^2 - \frac{2\mu}{\hbar^2} V_\alpha(r)\right] u_\alpha^J = \frac{2\mu}{\hbar^2} \sum_{\alpha'} V_{\alpha,\alpha'}^J u_{\alpha'}^J(r) \tag{5}$$

where

$$k_\alpha^2 = \frac{2\mu E_n}{\hbar^2} \tag{6}$$

If the incident channel is denoted by α one can rewrite Eq. (5) as

$$\left[\frac{d^2}{dr^2} - \frac{l(l+1)}{r^2} + K_\alpha^2 - \frac{2\mu}{\hbar^2} V_\alpha(r)\right] u_{\alpha\alpha}^J = \frac{2\mu}{\hbar^2} \sum_{\alpha'} V_{\alpha,\alpha'}^J u_{\alpha'\alpha}^J(r) \tag{7}$$

If the exit channel is denoted by β and $\beta \neq \alpha$, Eq. (5) becomes

$$\left[\frac{d^2}{dr^2} - \frac{l(l+1)}{r^2} + K_\alpha^2 - \frac{2\mu}{\hbar^2} V_\alpha(r)\right] u_{\alpha\beta}^J = \frac{2\mu}{\hbar^2} \sum_{\alpha'} V_{\alpha,\alpha'}^J u_{\alpha'\beta}^J(r) \tag{8}$$

Here the approximation of the inelastic channels being weakly coupled to the elastic channel is made, thus we have

$$u_{\alpha\beta}^J << u_{\alpha\alpha}^J \qquad \beta \neq \alpha \tag{9}$$

In terms of this approximation, the nuclear reaction matrix element can be written as:

$$S_{\alpha\beta}^J = -\frac{2\mu}{\hbar^2} \frac{1}{2ik_\alpha} \int_0^\infty u_{\alpha\alpha}^J(r) V_{\alpha\beta}^J(r) u_{\beta\beta}^J(r) dr \qquad \beta \neq \alpha \tag{10}$$

By use of the radial wave functions $u_{\alpha\alpha}^J$ and $u_{\beta\beta}^J$ obtained from the spherical optical model calculation, we can get the nondiagonal matrix elements from Eq. (10). The diagonal matrix element can be obtained directly from the spherical optical model calculation. Therefore, the direct inelastic scattering data of collective excitation can be calculated by the nuclear reaction matrix elements mentioned above. This method is named DWBA used for direct inelastic scattering of collective excitation.

2 CALCULATED RESULTS AND ANALYSES

For n+^{56}Fe reaction the following optical potential parameters were used:

$$V = 54.887 - 0.5532E + 0.003432E^2 - 24(N-Z)/A \tag{11}$$

$$W_S = 12.096 - 0.3938E - 12(N-Z)/A$$

or zero, whichever is greater, (12)

$$W_V = -0.1892 + 0.1750E - 0.001804E^2$$

or zero, whichever is greater, (13)

$$U_{SO} = 6.2 \tag{14}$$

$$r_R = 1.2027 \quad r_I = 1.3048 \quad r_{SO} = 1.2027 \tag{15}$$

$$a_R = 0.6930 \quad a_I = 0.4918 \quad a_{SO} = 0.6930 \tag{16}$$

The second order deformed parameter β_2 of the first excitation state 2^+ at 0.8468 MeV for ^{56}Fe is taken as 0.252[4].

For n+^{238}U reaction the following optical potential parameters[5] were chosen:

$$V = 47.5 - 0.3E \tag{17}$$

$$W_S = \begin{cases} 2.7 + 0.4E & E \leqslant 10 \text{ MeV} \\ 6.7 & E > 10 \text{ MeV} \end{cases} \tag{18}$$

$$W_V = 0.0 \tag{19}$$

$$U_{SO} = 7.5 \tag{20}$$

$$r_R = 1.24 \quad r_I = 1.26 \quad r_{SO} = 1.24 \tag{21}$$

$$a_R = 0.62 \quad a_I = 0.58 \quad a_{SO} = 0.62 \tag{22}$$

The second order deformed parameter β_2 of the first excitation state 2^+ at 0.0449 MeV for ^{238}U is taken as 0.216.

The direct inelastic scattering data for the first excitation state of ^{56}Fe and ^{238}U at incident neutron energies 14.0 and 20.0 MeV were calculated by CCOM code[6] and DWUCK4 code[7], respectively. In coupled–channel calculations, the coupling between the first excitation state and ground state was considered only. In order to express the relative deviation between the calculated results by CCOM and DWUCK4 codes, one defines a relation as

$$\Delta = \frac{\sigma^{(1)}_{\text{DWBA}} - \sigma^{(1)}_{\text{CCOM}}}{\sigma^{(1)}_{\text{CCOM}}} \tag{23}$$

Table 1 The calculated direct $\sigma_{n,n'}$ and relative deviations Δ

	^{56}Fe			^{238}U		
E_n	$\sigma^{(1)}_{CCOM}$	$\sigma^{(1)}_{DWBA}$	Δ	$\sigma^{(1)}_{CCOM}$	$\sigma^{(1)}_{DWBA}$	Δ
(MeV)	(b)	(b)		(b)	(b)	
14.0	0.07303	0.08800	20.5%	0.3029	0.4499	48.5%
20.0	0.08288	0.09770	17.9%	0.2571	0.3556	38.3%

The calculated inelastic scattering cross sections by CCOM theory and DWBA method as well as relative deviations are given in table 1. The first excitation state of ^{56}Fe is rather high, therefore, it is in the situation of weak coupling between the elastic and inelastic channels. From table 1 one can see that the relative deviations between two methods are 20.5% and 17.9% at energies 14.0 and 20.0 MeV, respectively. Figs. 1 and 2 show the comparisons of the calculated direct inelastic scattering angular distributions of the first excitation state of ^{56}Fe at eneries 14.0 and 20.0 MeV. One can see that the curve shapes obtained by two kinds of theories are very similar. The first excitation state of ^{238}U is rather low, therefore it is in the situation of strong coupling between the elastic and inelastic channels. From table 1 one can see that the relative deviations are 48.5% and 38.3% at energies 14.0 and 20.0 MeV, respectively. Figs. 3 and 4 show the comparisons of the calculated direct inelastic scattering angular distributions of the first excitation state of ^{238}U at energies 14.0 and 20.0 MeV by the two approaches. Although the curve shapes are also similar, the deviations of the absolute values are rather large.

3 SUMMARY

In this paper, the direct inelastic scattering cross sections and angular distributions for the first excitation states of ^{56}Fe and ^{238}U at incident neutron energies 14.0 and 20.0 MeV were calculated by CCOM theory and DWBA method. The calculated results show: 1. For ^{56}Fe, the DWBA method for calculating the direct inelastic scattering data is a reasonable approximation. 2. For large deformation nucleus ^{238}U, the DWBA method is not suitable and it is better to use the coupled–channel theory for the direct inelastic scattering data calculation. 3. The difference of the calculated results by two methods becomes little as incident neutron energy increases, it is because the perturbation theory DWBA is a good approach in high energy region. 4. The calculated inelastic

scattering data by DWBA method are always greater than those by coupled–channel theory in our calculations, it is mainly because the wave functions of DWBA method are calculated by spherical optical model, in which the influence of inelastic channel on elastic channel is neglected.

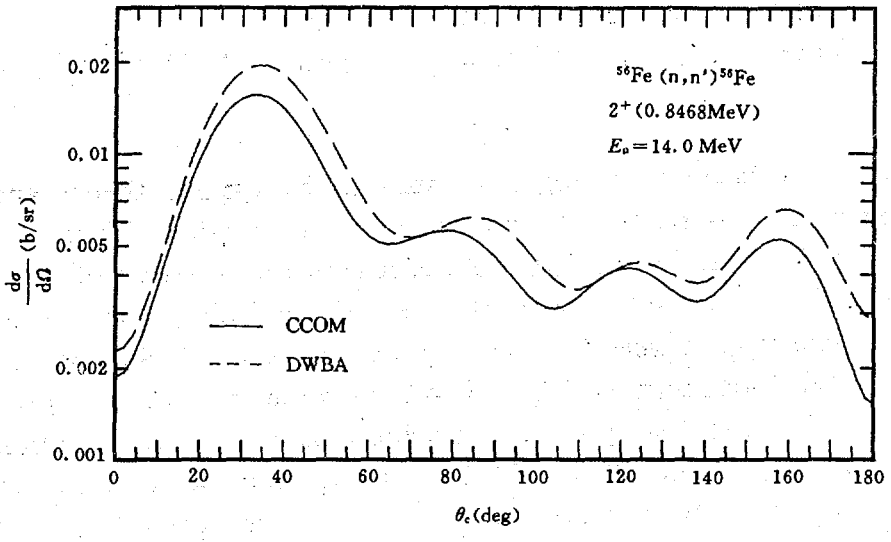

Fig. 1 Comparisón of the calculated direct $\sigma_{n,n}(\theta)$ of the first excitation state of ^{56}Fe at 14.0 MeV

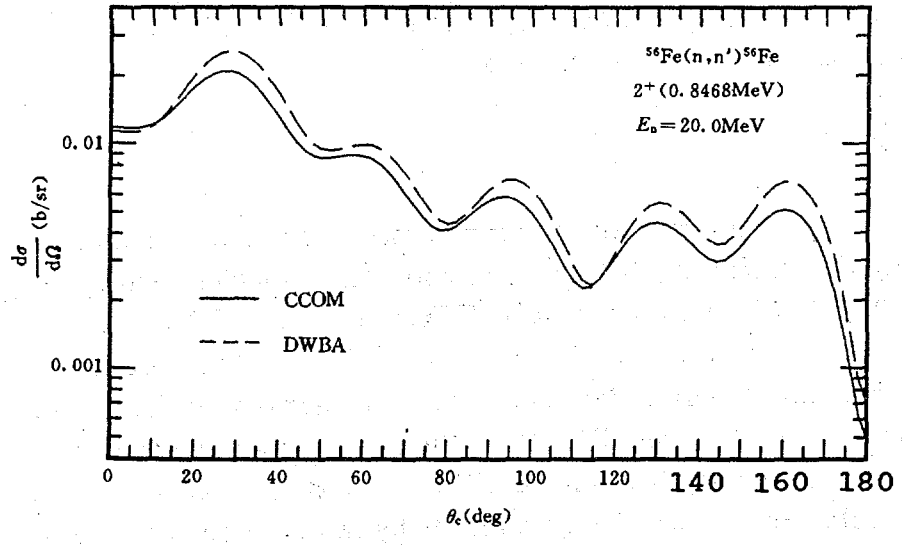

Fig. 2 The same as Fig. 1 except for 20.0 MeV

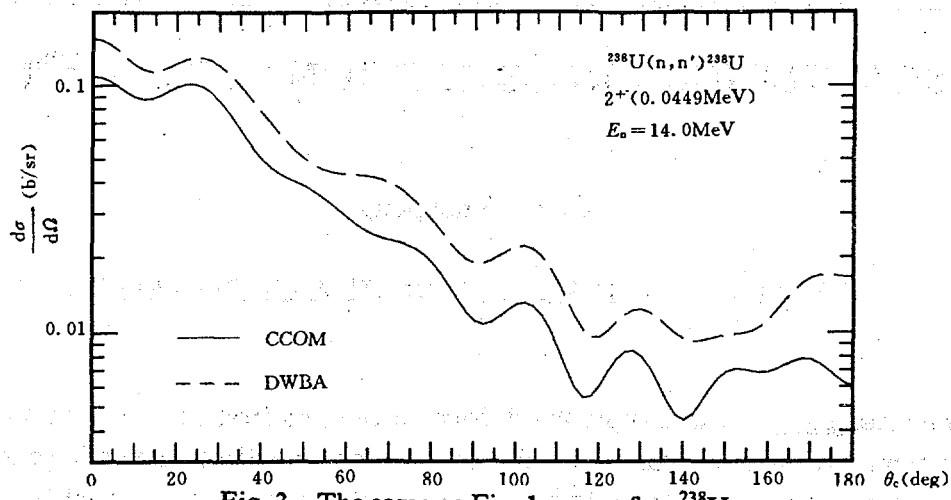

Fig. 3 The same as Fig. 1 except for ^{238}U

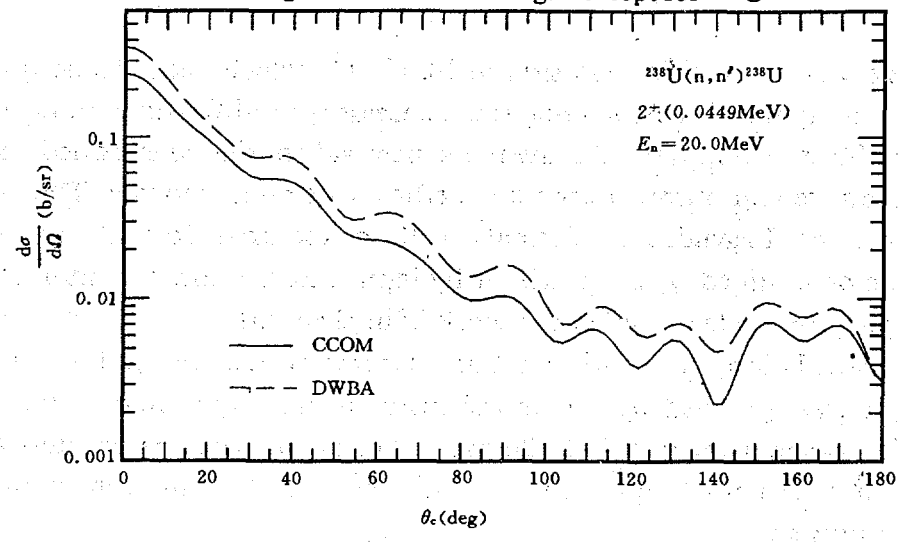

Fig. 4 The same as Fig.1 except for ^{238}U at 20.0 MeV

REFERENCES

[1] T. Tamura, Rev. Mod. Phys., 37, 679(1965)

[2] G. R. Satchler, "Direct Nuclear Reactions", Clarendon Press, Oxford, (1983)

[3] P. E. Hodgson, "Nuclear Reactions & Nuclear Structure", Clarendon Press, Oxford, p. 67, (1971)

[4] S. Mellema et al., Phys. Rev., C33, 481(1986)

[5] Ch. Lagrange, JAERI-M 5984, 1975, p. 58; Ch. Lagrange et al., Nucl. Sci. Eng., 83, 396(1983)

[6] Yang Zesen, High Energy Phys. & Nucl. Phys., 4, 778(1980)

[7] P. D. Kunz, "Distorted Wave Code DWUCK4", University of Colorado

THE CALCULATION OF DIRECT INELASTIC SCATTERING CROSS SECTION FOR n + ^{238}U

Chen Zhenpeng

(DEPART. OF PHYSICS, TSINGHUA UNIVERSITY)

The nucleus ^{238}U is a typically deformed one, its first several levels belong to a typically rotational band. In order to calculate the direct inelastic scattering cross section of neutron for n+^{238}U, coupled–channel optical model has to be used.

The code used is the CDC–version of ECIS79[1], which needs to be run in CRAY super computer. We have done some necessary modifications to make it to be run in VAX–computer. Meanwhile a new subroutine was added to it, which can produce and output Legendre coefficients simultaneously. The maximum number of Legendre coefficients with a required format by code UNF[2]can be determined by S–matrix or by input file. So now it is more convenient for using the code in evaluation work of nuclear data.

In this calculation, the optical model parameter set was got by Tang Guoyou[3]. It was obtained by a comprehensive fitting experimental data for n+^{238}U, which range from 10 keV to 20 MeV. The geometrical parameters and depths of optical potential which change with energies E of incident neutron are given as follows :

$R_r = R_{so} = 1.26840$ fm, $\quad a_r = a_{so} = 0.60200$ fm
$R_v = R_s = 1.35090$ fm, $\quad a_v = a_s = 0.50470$ fm

$V_r(e) = 44.2784 - 0.4387E + 0.01424E^2 - 24(A-2Z)/A$ (MeV)
$W_v(e) = 1.4504 - 0.03514E$ (MeV)
$W_s(e) = 3.7833 + 0.1521E$ (MeV)
$V_{so} = 6.2$ (MeV)

The deformation parameters are $\beta_2 = 0.240$, $\beta_4 = 0.057$.

From the view of theory, if a set of spherical optical model parameters is used in coupled–channel calculation, the imaginary part of potential should be decreased for improving the final result. We finded that at 4.25 MeV, when the

potential depthes were decresed about 30 percent, the inelastic scattering cross sections at 2^+ and 4^+ levels increased about 20 percent. It seems rather sensitive for them; but the elastic cross section just changes a little. Due to the parameters of Tang will be used in whole evaluation of $n+^{238}U$, we did not change them any more in this calculation.

A primary calculation shown that the direct inelastic scattering cross section at level 10^+ is very small. So the coupling schem involves only the first 5 levels, that is 0^+, 2^+, 4^+, 6^+, 8^+. The positions exist at 0.0, 0.04489, 0.1484, 0.3072 and 0.5178 MeV, respectively. It has been pointed out[4] that the calculation result is sensitive to the coupling schem used in some extent. The calculation shown that when coupling schem (0^+, 2^+, 4^+) was employed at 4.25 MeV, the inelastic cross section at 2^+ level increased about 15 percent than before, 50 percent for 4^+ level. It seems rather sensitive too. We think that it is good enough to take coupling schem (0^+, 2^+, 4^+, 6^+, 8^+).

The calculation was proceeded continuously in 20 energies ranging from 0.005 MeV to 20 MeV. The output includes all the integrated and differential cross sections and Legendre coefficients. The CPU time is about 3 hours.

It's very difficult to make a comparison between calculation values and experimental data at low energies due to the compound nucleus contribution. There are no experimental data in high energies larger than 3.5 MeV. So further calculation which includes H–F modification has to be done.

REFERENCES

[1] Chen Zhenpeng, Summary report of ECIS79. (1992)

[2] Zhang Jingshang, Communication of Nuclear Data Progress, No. 7, 14(1992)

[3] Tang Guoyou, Communication of Nuclear Data Progress, No. 6, 279(1991)

[4] J. P. Delaroch et al., Nuclear Theory in Nuclear Data Evalution, V–1, p. 257 (1975)

CALCULATION OF PROTON INDUCED REACTIONS ON ^{89}Y IN $E<$ 40 MeV ENERGY REGION

Shen Qingbiao Zhao Wenrong

(CHINA INSTITUTE OF ATOMIC ENERGY, BEIJING)

Cai Chonghai

(DEPART. OF PHYSICS, NANKAI UNIVERSITY, TIANJIN)

ABSTRACT

A set of proton optical potential parameters for $E<$ 40 MeV was obtained based on the available experimental data of ^{89}Y and neighbour nucleus ^{90}Zr. The calculated nuclear data are in good agreement with the experimental data for some channels, for which there exist better measured values. The calculated radioisotope yield cross sections show us which energy region is more suitable for specific radioisotope production in certain nuclear reaction.

INTRODUCTION

The studies of charged particle induced reaction in $E<$ 50 MeV energy region are significant for the applications of nuclear data, such as the medical radioisotope production, and for the fundamental researches, such as the studies of radioactive nuclear beams.

The cross sections of nuclear reactions are needed to determine the optimum energy range of a production process, i. e. the energy range which gives the maximum yield of the desired radioisotope and the minimum yields of impurities. At low projectile energies ($E<$20 MeV), the number of open reaction channels is generally small. With increasing projectile energy, the number of competing reaction channels increases and the demands on nuclear data information also increase.

It should be pointed out that in the interactions of intermediate energy par-

ticles with medium and heavy mass nuclei, not only neutron emission reactions but also processes involving emission of charged particles occur. The range of isotopic and non–isotopic products is thus broad. The non–isotopic impurities can be removed by chemical separations, the level of isotopic impurities is checked and suppressed only by a careful selection of the projectile energy range, i. e. through an accurate knowledge of cross sections.

In this paper taking proton induced reactions on ^{89}Y for $E<$ 40 MeV as example, the calculations and analyses are finished recently with the program CMUP2.

1 THEORIES AND PARAMETERS

We used optical model, evaporation model, and preequilibrium emission theory exciton model in the calculations. We chose the multi particle and hole state densities for which the Pauli exclusion principle[1~4] was considered. For composite particle emission, the pick–up mechanism of cluster formation[5~7] was used. The preequilibrium mechanism and the pick–up mechanism of composite particle emission were applied in the first, second, and third particle emission processes.

With program APCOM[8], the best charged particle optical potential parameters were searched automatically in fitting experimental nonelastic cross sections and elastic scattering angular distributions. With program CMUP2[9], the data for all reactions up to 50 MeV were calculated. The Gilbert–Cameron level density formula[10] was adopted.

For p+^{89}Y reaction, the excitation functions of the reactions $^{89}Y(p,n)^{89}Zr$, $^{89}Y(p,2n)^{88}Zr$, and $^{89}Y(p,pn+d)^{88}Y$ have been well measured from threshold to 40 MeV[11~14]. Based on these experimental data, we made the calculations of various nuclear data for this reaction.

Since the proton experimental nonelastic cross section and elastic scattering angular distribution of ^{89}Y are not available, the measured cross sections for all reaction channels of ^{89}Y were added together to obtain the nonelastic cross sections in proton energies lower than 22 MeV and then some corrections were made based on the calculated results by universal proton optical potential to those reaction channels, for which there are no any experimental data. When E_p is higher than 22 MeV, the measured nonelastic cross sections of the neighbour nucleus ^{90}Zr were applied, and a smooth connection was made between the two sets of nonelastic cross sections. There exist the measured nonelastic cross sections at energies 14.5, 30 and 40 MeV[15] and elastic scattering angular distributions at energies 22.5[16] and 40 MeV[17] for ^{90}Zr. We ob-

tained a set of proton optical potential parameters through fitting the experimental data for nuclei ^{89}Y and ^{90}Zr as follows :

$$V = 62.381 - 0.3743E - 0.005439E^2 + 24(N-Z)/A + 0.4Z/A^{1/3} \quad (1)$$

$$W_s = 11.661 - 0.2491E + 12(N-Z)/A$$

or zero, whichever is greater, (2)

$$W_v = -2.638 + 0.3211E + 0.001829E^2$$

or zero, whichever is greater, (3)

$$V_{so} = 6.2 \quad (4)$$

$$r_r = 1.168,\ r_s = 0.908,\ r_v = 1.338,\ r_{so} = 1.01,\ r_c = 1.251, \quad (5)$$

$$a_r = 0.5223,\ a_s = 0.5096 + 0.7(N-Z)/A$$

$$a_v = 0.5117 + 0.7(N-Z)/A,\quad a_{so} = 0.75. \quad (6)$$

Using proton optical potential parameters obtained above, adjusting the optical potential parameters of neutron and the other charged particles, and taking the free parameter of the square of the average two-body interaction matrix element $K = 630$ MeV^3, the calculated excitation functions for the reactions of ^{89}Y(p,n)^{89}Zr, ^{89}Y(p,2n)^{88}Zr, and ^{89}Y(p,pn+d)^{89}Y are in good agreement with the experimental data. Meanwhile, many kinds of nuclear data of ^{89}Y are predicted in the calculations.

2 CALCULATED RESULTS AND ANALYSES

In Fig. 1, the calculated nonelastic cross sections of ^{90}Zr are shown. They are in good agreement with the experimental data. Fig. 2 shows that the calculated proton elastic scattering angular distribution of ^{90}Zr at 22.5 MeV agrees with the experimental data pretty well. However, in Fig. 3 the calculated proton elastic scattering angular distribution of ^{90}Zr at 40 MeV only roughly agrees with the experimental data. These calculated results of ^{90}Zr show that one can use the proton optical potential parameters obtained above on neighbour nucleus of ^{89}Y.

The theoretical curves in the energy range from threshold to 40 MeV for three reactions of ^{89}Y(p,n)^{89}Zr, ^{89}Y(p,2n)^{88}Zr, and ^{89}Y(p,pn+d)^{88}Y are shown in Figs. 4~6 with measured results[11~14] together, respectively. The agreement between the theoretical curves and experimental data are excellent for ^{89}Y(p,n)^{89}Zr and ^{89}Y(p,2n)^{88}Zr reactions in the whole energy range. The calculated value is a bit higher than the measured results below 29 MeV

for $^{89}Y(n,pn+d)^{88}Y$ reaction. One can see clearly from Figs. 4 to 6 that the measured results by Saha et al.[11] are not reliable.

Above results show that for the reaction channels, for which there exist better measured data, we obtained rather good calculated results in agreement with the experimental data. Therefore, one can predict the nuclear data to those reaction channels for which there are nearly no reliable experimental data.

Fig. 7 shows the calculated n, p, d, t, ^{3}He and α emission cross sections induced by proton below 40 MeV.

Fig. 8 illustrates the calculated neutron multiplicity $M_{p,n}$ of ^{89}Y induced by proton below 40 MeV. One can see clearly that when $E_p < 13.5$ MeV $M_{p,n}$ equals 1.0 because all channels emitting two or three neutrons are not opened. $M_{p,n}$ may approach 1.7 after (p,2n) channel opened and $M_{p,n}$ may approach 1.95 after (p,3n) channel opened. Generally speaking, the higher the proton energy, the larger the neutron multiplicity. The calculated results also show that the maximum multiplicity in $E < 40$ MeV energy region for 5 kinds of charged particles is only a little larger than 1.0.

Fig. 9 illustrates the calculated yield cross sections induced by proton below 40 MeV. Many isotopes of the elements Zr, Y, Sr, Rb, and Kr can be produced in reaction p+^{89}Y. It is clear that the higher the proton energy, the larger the number of yield nuclei. Fig. 9 shows that if one wants to produce radioisotope ^{89}Zr it is better to choose the energy range of 7~15 MeV in reaction p+^{89}Y and in this case the impurity is not severe. If one wants to produce ^{88}Zr, ^{87}Zr, and ^{88}Y in reaction p+^{89}Y, it is better to choose the energy range of 15~30 MeV, above 30 MeV, and above 18 MeV, respectively.

3 CONCLUSIONS

Based on the available experimental data of ^{89}Y and neighbour nucleus ^{90}Zr, we obtained a set of proton optical potential parameters for $E < 40$ MeV. Then adjusting neutron and the other charged particle optical potential and level density parameters as well as taking the free parameter of the square of the average two-body interaction matrix element $K = 630$ MeV^3, the calculated nuclear data for some channels, for which there exist better measured data, are in good agreement with the experimental data in above mentioned energy region. The various predicted cross sections, yields, angular distributions, and emitted particle energy spectra in this energy region are reliable to some extent. The calculated radioisotope yield cross sections can tell us which energy region is more suitable for specific radioisotope production in certain nuclear reaction.

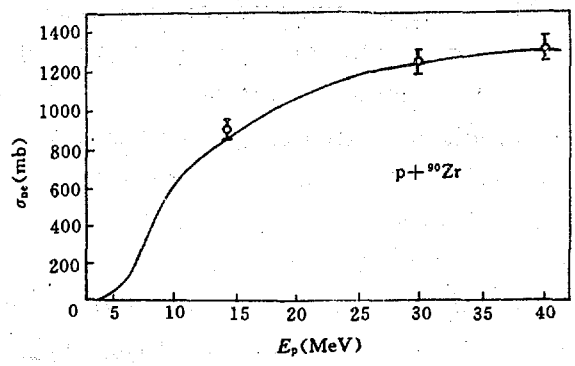

Fig. 1 Comparison of the calculated nonelastic cross sections of ^{90}Zr with experimental data

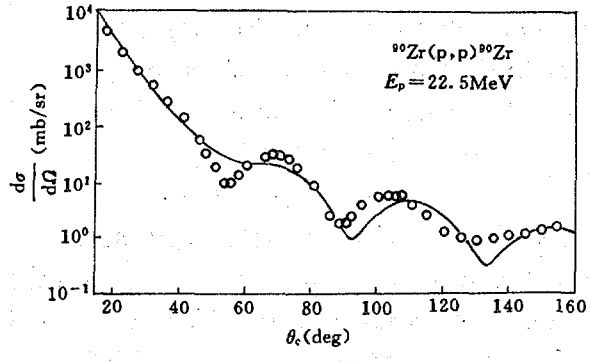

Fig. 2 Comparison of the calculated $\sigma_{p,p}(\theta)$ of ^{90}Zr at 22.5 MeV with the experimental data

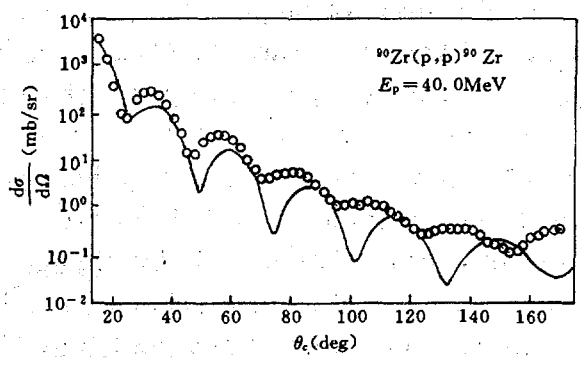

Fig. 3 The same as Fig. 2 except for 40 MeV

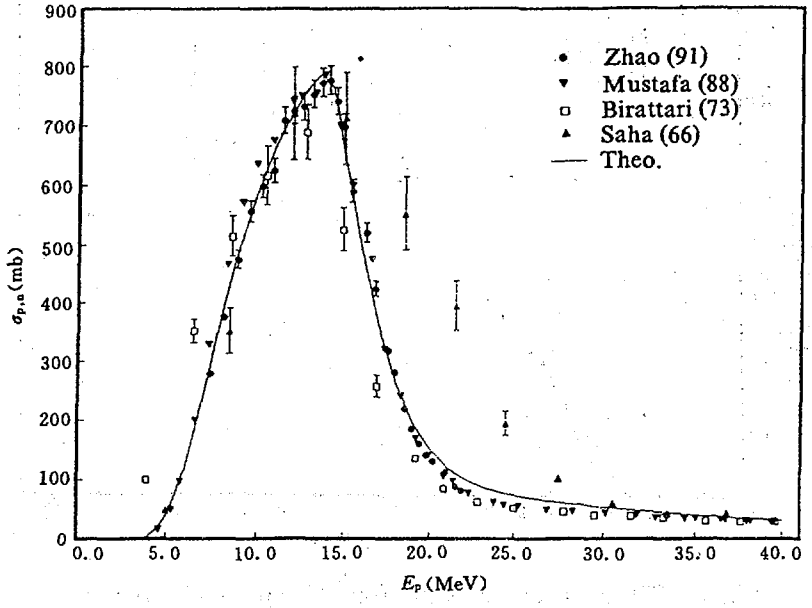

Fig. 4 Comparison of the calculated ^{89}Y $\sigma_{p,n}$ with the experimental data

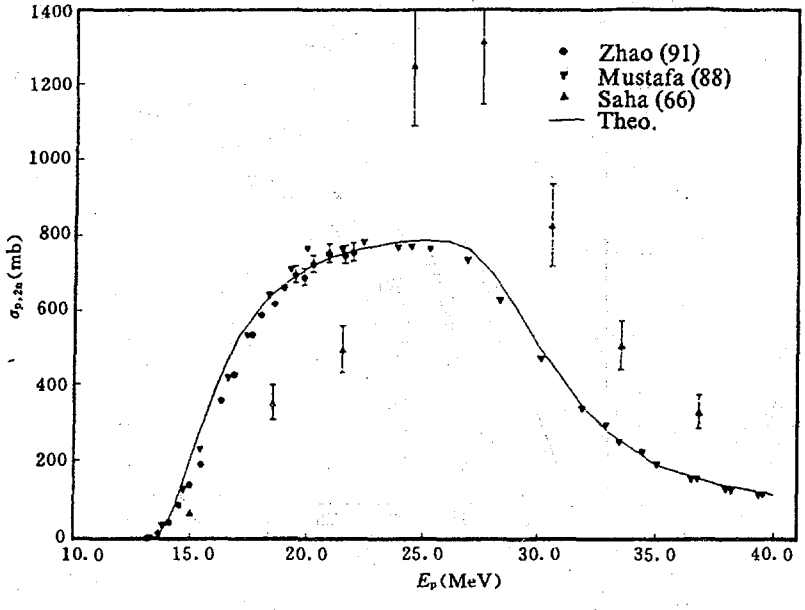

Fig. 5 The same as Fig. 4 but for $^{89}Y(p,2n)^{88}Zr$ reaction

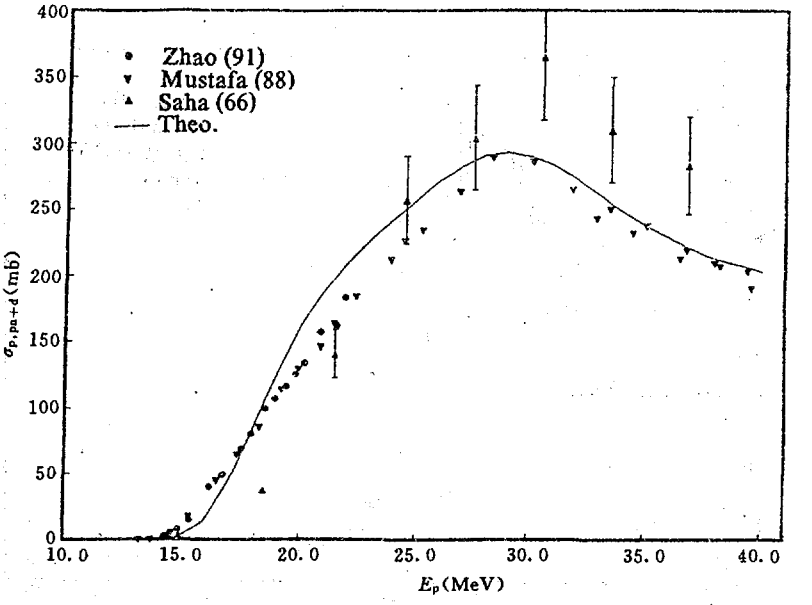

Fig. 6 The same as Fig. 4 but for $^{89}Y(p,pn+d)^{88}Y$ reaction

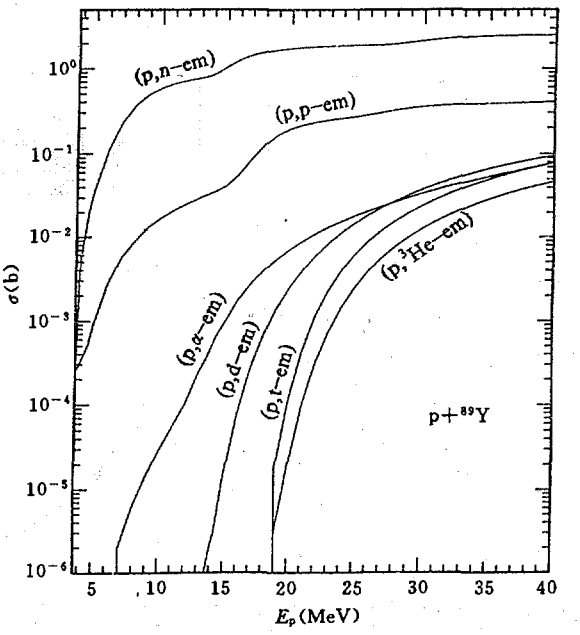

Fig. 7 The calculated proton induced emission cross sections for 6 particles below 40 MeV

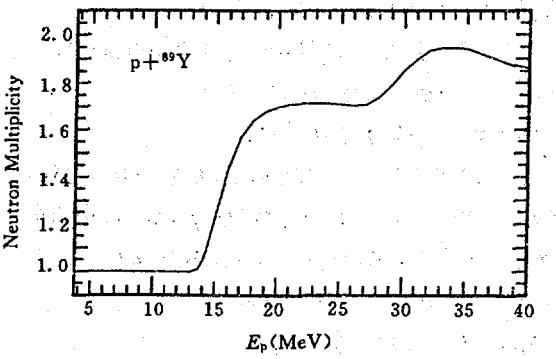

Fig. 8 The calculated neutron multiplicity of ^{89}Y induced by proton below 40 MeV

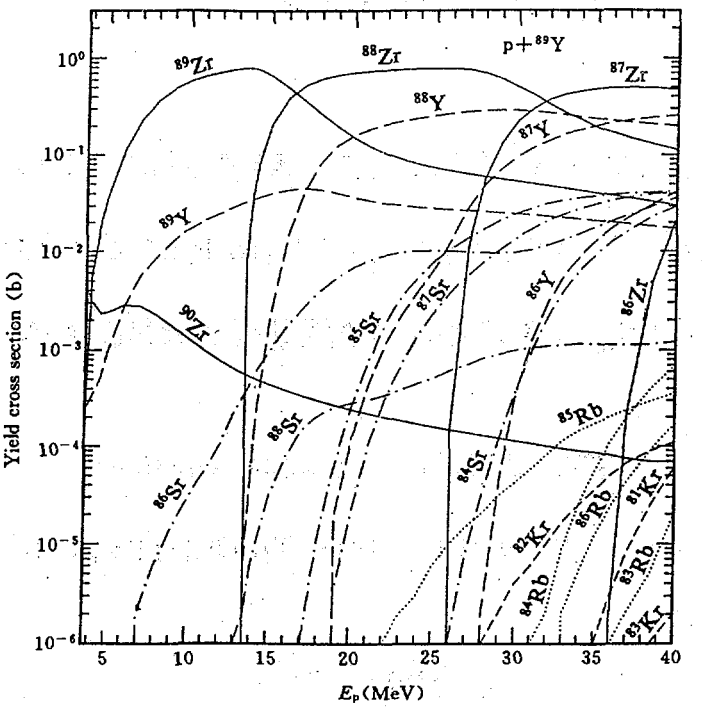

Fig. 9 The calculated yield cross sections in reaction p+^{89}Y below 40 MeV

REFERENCES

[1] M. Bohning, Nucl. Phys., A152, 529(1970)
[2] F. C. Willams, Nucl. Phys., A166, 231(1971)
[3] C. Kalbach, BNL-NCS-51694, p. 113, (1983)
[4] Zhang Jingshang et al., High Energy Physics & Nuclear Physics (China), 13, 822(1989)
[5] A. Iwamoto et al., Phys. Rev., C26, 1821(1982)
[6] K. Sato et al., Phys. Rev., C28, 1527(1983)
[7] Zhang Jingshang et al., Commun. in Theor. Phys., 10, 33(1988)
[8] Shen Qingbiao et al., Commu. Nucl. Data Progress, 7, 41(1992)
[9] Cai Chonghai et al., Nucl. Sci. Eng., (to be published)
[10] A. Gilbert et al., Can. J. Phys., 43, 1446(1965)
[11] G. B. Saha et al., Phys. Rev., 144, 962(1966)
[12] C. Birattari et al., Nucl. Phys., A201, 579(1973)
[13] M. G. Mustafa et al., Phys. Rev., C38, 1624(1988)
[14] Zhao Wenrong et al., Chin. J. Nucl. Phys., 14, 7(1992)
[15] W. Bauhoff, Atom. Data and Nucl. Data Tables, 35, 429(1986)
[16] J. B. Ball et al., Phys. Rev., 135B, 706(1964)
[17] L. N. Blumberg et al., Phys. Rev., 147, 812(1966)

CALCULATION OF VARIOUS CROSS SECTIONS FOR p+^{241}Am REACTION IN 5.5~35 MeV ENERGY REGION

Shen Qingbiao Zhuang Youxiang

(CHINESE NUCLEAR DATA CENTER, IAE)

ABSTRACT

The calculations of various cross sections for p+^{241}Am reaction in 5.5~35 MeV energy region were made with CFUP1 program. For (p,F) and (p,2n) reactions, the calculated results agree with the available experimental data pretty

well. The predicted cross sections have a significant reference value.

INTRODUCTION

The study of light charged particle induced reaction on fissile nuclei is one of the important subjects. Based upon the Bohr–Wheeler formalism[1], Arthur and Young have made the calculations of the fission cross sections of ^{238}U and ^{237}Np induced by neutrons and protons below 100 MeV with GNASH program[2]. In order to calculate the neutron or charged particles (p, d, t, ^{3}He, α) induced reactions on the fissile nuclei , a program CFUP1 in the incident energy range up to 35 MeV is developed within the framework of optical model, preequilibrium statistical theory based on the exciton model, and the evaporation model. In the first, second, and third particle emission processes, preequilibrium emission and the evaporation are included; in the fourth and fifth particle emission processes, evaporation is considered only. The output data of CFUP1 include: 1. The cross sections and ν values: σ_{tot} and σ_{el} (only for neutron as projectile), as well as σ_{non} , $\sigma_{x,\gamma}$, $\sigma_{x,n}$, $\sigma_{x,2n}$, $\sigma_{x,3n}$, $\sigma_{x,4n}$, $\sigma_{x,5n}$, $\sigma_{x,np}$, $\sigma_{x,p}$, $\sigma_{x,d}$, $\sigma_{x,t}$, $\sigma_{x,^3He}$, $\sigma_{x,\alpha}$, $\sigma_{x,f}$, $\sigma_{x,n'f}$, $\sigma_{x,2nf}$, $\sigma_{x,3nf}$, $\sigma_{x,4nf}$, $\sigma_{x,pf}$, $\sigma_{x,F}$ (total fission cross section), and the ν values of various fission processes. 2. The elastic scattering angular distributions and the ratios of the elastic scattering differential cross section to Rutherford scattering differential cross section. 3. The energy spectra of all secondary particles in one to five particle emission processes and the fission neutron spectra of various fission processes.

The purpose of this paper is to calculate various cross sections for $p+^{241}Am$ reaction in 5.5~ 35 MeV energy region. Up to now, the cross sections of (p,F) and (p,2n) channels between 8 and 16 MeV have only been measured[3]. If the reasonable model parameters are chosen and the calculated (p,F) and (p,2n) cross sections agree with the experimental data pretty well, the nuclear data for which there are no any experimental data can be predicted reasonably.

1 THEORIES AND PARAMETERS

The multi particle and hole state densities considered the Pauli exclusion principle in the exciton model[4~7] are chosen.

In the evaporation model, the fission width of the compound nucleus is calculated by Bohr channel theory with effect single peak fission barrier:

$$\Gamma_f = \frac{1}{2\pi\rho(Z,A,U)} \int_0^\infty \frac{\rho_f(Z,A,x)}{1+\exp[\frac{2\pi}{\hbar\omega}(x+V_f-U)]}\mathrm{d}x \tag{1}$$

where V_f is the fission barrier. The formula of level density on saddle point is as following as described in Ref. [8].

$$\rho_f = \frac{K_1\sqrt{\pi}\exp[2\sqrt{a(U_x+K_2)}+\frac{(x-U_x-\Delta)}{T}]}{12\sqrt{a(U_x+K_2)}\,U_x}, \quad \text{if } x \leqslant U_x+\Delta \tag{2}$$

$$\rho_f = \frac{K_1\sqrt{\pi}\exp[2\sqrt{a(U_e+K_2)}]}{12\sqrt{a(U_e+K_2)}\,U_e}, \quad \text{if } x > U_x+\Delta \tag{3}$$

where

$$T = [\sqrt{\frac{a}{U_x+K_2}} - \frac{1}{U_x} - \frac{0.5}{U_x+K_2}]^{-1} \tag{4}$$

$$U_x = U_c + U_a/A \tag{5}$$

$$U_e = x-\Delta \tag{6}$$

K_1 and K_2 are adjustable parameters. The ν value of the fission process is calculated by Howerton's semi-classical formula[9].

For composite particle emission in exciton model, the pick-up mechanism of cluster formation[10~12] is used in the first particle emission process. The Gilbert-Cameron level density formula[13] is applied in program CFUP1. The inverse cross sections of the emitted particles used in statistical theory are calculated by the optical model. In the optical model calculation, the phenomenological optical potential form of Becchetti and Greenlees[14] is adopted.The partial widths for γ-ray emission are calculated on the basis of the giant dipole resonance model with two resonance peaks.

According to Bohr postulation the decay of a compound nucleus is indepent of its formation, some statistical theory parameters obtained in calculations of reactions induced by neutrons on neighbor nucleus ^{240}Pu[15] are used in calculations of p+^{241}Am reaction. Some universal optical potential and level density parameters are adopted. In order to fit (p,F) experimental data, some proton optical potential parameters are adjusted in our calculation. In order to

make calculated (p,2n) cross sections in agreement with experimental data, the exciton model constant $K=980$ is taken and some neutron optical potential parameters are adjusted in reasonable region.

2 CALCULATED RESULTS AND ANALYSES

The calculated various cross sections for p+^{241}Am reaction in 5.5~35 MeV energy region and the comparison of the calculated curves with experimental data for (p,F) and (p,2n) channels are shown in Fig. 1. It is evident that the calculated (p,F) and (p,2n) cross sections are in pretty good agreement with the experimental data. The cross sections of all the possible reactions in the energy region are predicted: (non), (p,F), (p,f), (p,nf), (p,2nf), (p,3nf), (p,4nf), (p,pf), (p,n), (p,2n), (p,3n), (p,4n), (p,5n), (p,np), (p,p′), (p,d), (p,t), (p,^{3}He), and (p,α). Considered the theories and parameters used in our calculations are reasonable, the predicted cross sections have significant reference value.

The calculated results show that the nonelastic cross sections are mainly contributed from the fission cross section. When incident energy is larger than 15 MeV, the (p,pf) cross section has evident contribution. It seems that the (p,df), (p,tf), ··· cross sections can not be neglected although they are not included in program CFUP1. When incident energy is less than 20 MeV, (p,n) and (p,2n) cross sections are main particle emission cross sections. The light charged particle emission cross sections become important when the incident energy is larger than 20 MeV. Further study to this subject should be done as more experimental data are available.

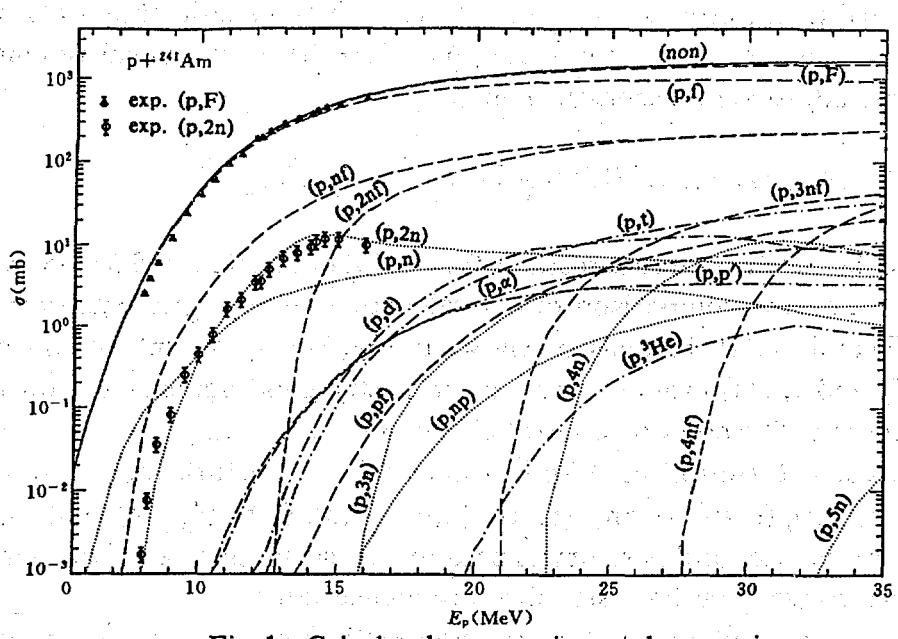

Fig. 1 Calculated cross sections and comparison with the experimental data of $\sigma_{p,F}$, $\sigma_{p,2n}$

REFERENCES

[1] N. Bohr et al., Phys. Rev., 56, 426(1939)

[2] E. D. Arthur et al., 50 Years with Nuclear Fission, April 25～28, Washington, Vol. 2, p. 931, (1989)

[3] V. Metag et al., Nucl. Phys., A213, 397(1973)

[4] M. Bohning, Nucl. Phys., A152, 529(1970)

[5] F. C. Williams, Nucl. Phys., A166, 231(1971)

[6] C. Kalbach, BNL–NCS–51694, p. 113, (1983)

[7] Zhang Jingshang et al., High Energy Physics & Nuclear Physics, 13, 822(1989) (in Chinese)

[8] Zhang Jingshang et al., Collection of Theoretical Method on Nuclear Reactions & Their Applications, p. 226, (1980) (in Chinese)

[9] R. J. Howerton, Nucl. Sci. Eng., 62, 438(1977)

[10] A. Iwamoto et al., Phys. Rev., C26, 1821(1982)

[11] K. Sato et al., Phys. Rev., C28, 1527(1983)

[12] Zhang Jingshang et al., Commun. in Theor. Phys., 10, 33(1988)

[13] A. Gilbert et al., Can. J. Phys., 43, 1446(1965)

[14] F. D. Becchetti et al., Phys. Rev., 182, 1190(1969)
C. M. Perey et al., Atomic Data & Nuclear Data Tables, 17, 3(1976)

[15] Cai Dunjiu et al., CNDP, 6 Supplement, 84(1992)

INFLUENCE OF NUCLEAR DEFORMED FLUCTUATION ON PARTICLE EMISSION

Wang Shunuan

(CHINESE NUCLEAR DATA CENTER, IAE)

ABSTRACT

The influence of nuclear deformed fluctuation on the double differential cross section and spectrum of emitted particles is studied in a stochastic framework in detail in the early time regime prior to fission events especially for medium heavy nuclei with very high fission barrier by solving a coupled master equation and Fokker–Planck equation.

INTRODUCTION

The dynamical coupling of fission and light particle evaporation is usually described by a coupled Fokker–Planck equation for fission and master equation for particle evaporation in which the emission probabilities per unit time depend on the instantaneous value of the deformation coordinate of the nucleus [1, 2]. As pointed out in Ref. [3], it is a formidable work to get the solution of such a set of coupled Fokker–Planck equation and master equation. H. S. Wio et al.[3] studied the coupled dynamics of particle evaporation and fission in a stochastic framework first. The competition between evaporation and fission was described in the early time regime prior to fission events. In this regime the nuclear collective deformed fluctuation can be assumed essentially independent of the particle emission process, therefore a meaningful solution of a simplified coupled model can be obtained and the effect of the fluctuation on the statistical properties of particle evaporation can be described properly.

All the works mentioned above is based on a elemental physical idea, i. e. the internal motion or single particle motion degrees of freedom is assumed to be in equilibrium inside the saddle point of the excited nucleus. Then, a statistical model can be used to describe the light particle evaporation process. The Fokker–Planck equation can be used to describe the collective deformed motion at other degrees of freedom in equilibrium acting as a heat bath with tem-

perature T and causing thermal fluctuation. There is no any considering of the impact from the collective deformed motion process to the internal motion equilibrium process, especially in the case of near deformed ground state. As a matter of fact, from the physical point of view there should be a coupling between the internal and collective deformed motions degrees of freedom during the course of a incident particle absorption to a compound nucleus formation. Both internal single particle motion and collective deformed motion during the process undergo the stage from non–equilibrium to equilibrium, even various degrees of freedom in a nucleus relax at different rates, for example, the relaxation time for nucleonic degrees of freedom is short, the relaxation of collective deformed variable in nuclear fission is much longer[4]. In the present paper in order to consider the coupling between the internal and collective deformed motion degrees of freedom especially in the early time regime prior to fission or for medium heavy nuclei with very high fission barrier, or in other words, to consider the influence of the fluctuation of nuclear collective deformed motion degrees of freedom on particle emission process near deformed ground state, we introduce the fluctuation of nuclear collective deformed variable associated with the fission process as a external noise to a generalized master equation of exciton model including preequilibrium and equilibrium emission process. So far as we known, the basic idea of preequilibrium theory is based on that phase space can be divided up into many regions so that there is in local equilibrium in each of them but of course not necessarily between regions[4]. In exciton model, actually we have each stage in local equilibrium[5]. Hence, each stage can provide a heat bath and cause thermal fluctuation respectively to the collective deformed degrees of freedom during the internal single particle motion equilibrium process, then the acting of the fluctuation of collective deformed degrees of freedom on the particle emission process near deformed ground state occurs. Based on the idea described above, in the present paper we consider that the emission probability per unit time which relates with external space depends on the instantaneous value of the deformation coordinate of the nucleus. The exact closed form solution of the generalized master equation of exciton model including preequilibrium and equilibrium emission with the fluctuation can be used to get the double differential cross sections and energy spectrum of the emitted particle. Thus the effect of the nuclear collective deformed fluctuation near deformed ground state on the double differential cross section and energy spectrum of the emitted particle can be investigated in the stochastic framework in detail. We have that the model describing the influence of nuclear deformed fluctuation on particle emission as the following : in which the nuclear deformed fluctuation is governed by the Fokker–Planck equation for the distribu-

tion function of the collective coordinates and their conjugate momenta. The influence is entered in the generalized master equation of exciton model for the probability of finding the system describing the particle emission process. The particle emission process depends on the instantaneuos value of the deformation coordinate of the nucleus by means of the emission probability per unit time depending on the instantaneous value of the deformation coordinate of the nucleus. It can be assumed that in the early time regime prior nuclear collective deformed fluctuation is independent of the particle emission process and will be entered in the emission process as an external noise. With all of those considerations the formulation of the model is constructed and presented in section 1, the analysis and discussion are presented in section 2, respectively.

1 FORMULATION OF THE MODEL

We assume that the fission process is described by only one deformation variable q, and the friction of the system is large. Thus we have a Fokker–Planck equation in configaration space instead of phase space. We also assume that the reduced mass m and the friction constant β are independent of the deformation variable q as constant, and assume that the fission potential has the form of harmonic oscillator as usual[1, 2].

The Fokker–Planck equation has been studied in Ref. [6]. If the friction constant β is much larger, the equilibrium is reached very quickly in momentum space. Thus the Fokker–Planck equation can be simplified to Smoluckowski equation which has been studied in Ref. [6] too.

The Langevin equation associated with Smoluckowski equation has the form as bellow[6]

$$\frac{\mathrm{d}q(t)}{\mathrm{d}t} = -\frac{1}{\beta}\frac{\partial}{\partial q}(U_f(q)/m) + \xi(t) \tag{1}$$

here, $U_f(q)$ is the fission potential which has the form of harmonic oscillator. $\xi(t)$ is a Gassion white noise, its correlation function can be derived[7,8].

For time shorter than a characteristic time to over cross the fission barries or in the early time regime prior to fission,we consider the fluctuation in the first minimum of the potential only. Thus Eq. (1) can be reduced as

$$\frac{\mathrm{d}q(t)}{\mathrm{d}t} = -Aq(t) + \xi(t) \tag{2}$$

with $A = \frac{\omega_0^2}{\beta}$

here, ω_0 is the frequency of harmonic oscillator in the first minimum of the fission potential.

Assuming $q(t)$ obying Ornstein–Uhlenbeck process[8, 9], the correlation function of $q(t)$ can be obtained as in Refs. [8, 9].

The generalized master equation describing the particle emission reads as

$$\frac{\mathrm{d}}{\mathrm{d}t} p(n,\Omega,t) = \Sigma_{m=n-2,\Delta m=2}^{n+2} \lambda_{m\to n} \int p(m,\Omega',t) G(\Omega',\Omega) \mathrm{d}\Omega'$$

$$- (W(n) + \Sigma_{m=n-2,\ \Delta m=0,\pm 2}^{n+2} \lambda_{n\to m}) p(n,\Omega,t) \tag{3}$$

here, $p(n, \Omega, t)$ is the probability of finding the system in the state of exciton number n and direction Ω at time t. $G(\Omega, \Omega')$ is the distribution probability of two–nucleon collision from direction Ω to Ω' inside a nuclear matter. $W(n)$ is the total emission rate of the nth exciton state. $\lambda m \to n$ is the exciton transition rate from exciton number m to n. The exact closed form solution of Eq. (3) can be obtained[10] with the following as in Ref. [8]

$$w_n^i(\varepsilon) = \frac{2s_i + 1}{\pi^2 h^3} \mu_i p \frac{(n-1)}{gE^{n-1}} \varepsilon \sigma_i(\varepsilon) (E - U_f(q) - B_i - \varepsilon)^{n-2} \mathrm{d}\varepsilon \tag{4}$$

$$W_i(n) = \int_0^{E - Bi - Uf(q)} w_n^i(\varepsilon)\ \mathrm{d}\varepsilon \tag{5}$$

$$W(n) = \Sigma_i W_i(n)$$

Thus the double differential cross section and energy spectrum of the emitted particle for channel (a,b) can be expressed as shown in Ref. [10]

$$\frac{\mathrm{d}\sigma^2}{\mathrm{d}\varepsilon \mathrm{d}\Omega} = \sigma_a \Sigma_n w_n^b(\varepsilon) t(n,\theta) \tag{6}$$

$$\frac{\mathrm{d}\sigma}{\mathrm{d}\varepsilon} = \sigma_a \Sigma_n w_n^b(\varepsilon) 4\pi \zeta_0(n) \tag{7}$$

here, σ_a is a composite system formation cross section, $t(n,\theta)$ and ζo can be obtained by the exact closed form solution of Eq. (3)[10]. In generally, since the up limit of time integral of generalized master equation is to infinity and the sum over exciton number n is large enough so that the calculated results are contributed from both preequilibrium and equilibrium process, approximately.

At this point what we have seen clearly from Eqs. (4, 5) and Eq. (2) is that the parameter q of the Langevin equation has been coupled to the master equation to fluctuate the particle emission process by a kind of quadratic Ornstein–Uhlenbeck noise in the early time regime prior to fission.

For weak noise we assume that $q(t)$ is in the form of

$$q(t)^2 = < q(t)^2 > + \eta(t) \tag{8}$$

By means of the correlation function of $q(t)$ obying Ornstein–Uhlenbeck process we have[8]

$$q(t)^2 = D / A + \eta(t) \tag{9}$$

with $$D = \frac{kT}{\beta m}$$

where $\eta(t)$ is a weak fluctuation.

Thus we obtain the following in the range of first minimum of the fission potential:[8]

$$U_f(q(t)) = < U(q) > + 1 / 2m\omega_0^2 \eta(t) \tag{10}$$

with $$< U(q) > = kT / 2$$

It is worth to do that if the contribution of the noise term can be neglected in Eq. (10) for simplicity. We find that the influence of the fission potential $U_f(q)$ enters in Eq. (4) and (5) as $< U(q) >$ giving a finite nonvanishing contribution to the particle emission process. Thus Eq. (4) and (5) change to the form as

$$w_n^i(\varepsilon) = \frac{2s_i + 1}{\pi^2 h^3} \mu_i p \frac{(n-1)}{gE^{n-1}} \varepsilon \sigma_i(\varepsilon)[E - Bi - \varepsilon - (kT)n / 2]^{n-2} d\varepsilon \tag{11}$$

$$W_t(n) = \int_0^{E-Bi-\frac{1}{2}kT} w_n^t(\varepsilon)\ d\varepsilon \tag{12}$$

here, $(kT)n$ is the temperature of thermal bath in exciton number n stage which is in local equilibrium. For convenience, we take roughly the following at the present paper.

$$(kT)n \sim kT = (E/a)^{\frac{1}{2}}$$

here, a is a level density parameter of the compound nucleus. Actually, it is the lowest temperature among each stage of the composite system. Hence the lowest influence of the collective deformed fluctuation on particle emission can be estimated at least by means of this simple treatment.

At the present paper we consider the weak fluctuation only so that $\eta(t)$ term in Eq. (10) can be neglected. Therefore the influence of $< U(q) >$ on the double differential cross section and spectrum of the emitted particle can be analyzed properly[8].

If we consider the influence of the noise term $\eta(t)$ then the occupying probabilities $P(n, \Omega, t)$ of master equation should be a function of noise $\eta(t)$, and $P(n, \Omega, t)$ should be replaced by $P(n, \Omega, t, \eta(t))$. In order to have a sensible result what we need is an average of the occupying probability $P(n, \Omega, t, \eta(t))$ over a realistic $\eta(t)$.

2 ANALYSIS AND DISCUSSION

In the calculations we consider only the weak fluctuation by taking into account $< U(q) >$ term and neglecting the term with $\eta(t)$ in Eq. (10). We take ^{93}Nb(n,n′) reaction with incident energy E_n = 15, 30 MeV respectively as a example. The square of average two–body interaction matrix element K= 190 MeV^3 is used. The level density parameters are chosen from Ref. [11]. It can be seen clearly from Eqs. (11, 12) that when the excitation energy E goes up, the emission probabilities per unit time go down, and the influence of $< U(q) >$ on the spectrum of emitted particles is more obviously as shown in Fig. 1. Even for E_n = 15 MeV, the shape of the spectrum at higher and lower energy range shows a finite nonvanishing contribution by taking into account the influence of the nuclear deformed fluctuation. The fluctuation $< U(q) >$ occupies $kT/2$ energy so that the spectrum goes down at higher energy range and up at lower energy range. This means that the preequilibrium emission charac-

teristic is reduced somehow by considering the fluctuations. As mentioned in Sec. 1, $(kT)n \sim kT = (E/a)^{1/2}$ is taken in the calculation. If $(kT)n$ is taken as a function of exciton number n in some suitable way, the preequilibrium emission would be reduced more by considering the fluctuation because $(kT)n$ may be greater than kT.

The effect of the nuclear collective deformed fluctuation on statistical model can be used for some midium heavy nuclei data calculation in the energy range from 3 MeV to 40 MeV for needs of some applications. By using a statistical model including equilibrium and preequilibrium mechanism with the considering of the influence of the nuclear collective deformed fluctuations, not only a better fitting with cross sections but also a reasonable shape of spectrum in high energy tail and lower energy range could be obtained. More theoretical and experimental inverstigations are necessary to obtain more detailed results on the shape of emitted particle spectrum especially in lower and higher energy range.

It has been clearly recognized that it is a very interested subject in studying the coupled model of particle emission and fission. How to consider the couple between single particle motion and collective deformed motion degrees of freedom after a incident particle absorbing is still an interested open problem.

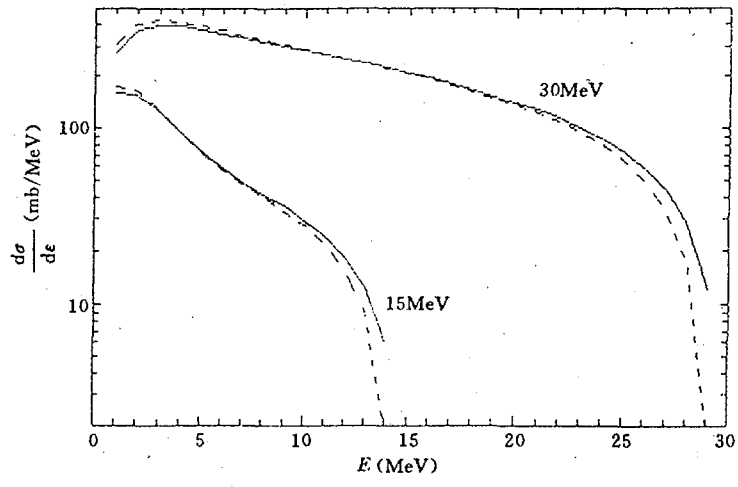

Fig. 1 The spectrum of ^{93}Nb(n,n′) reaction

– – – With the influence of nuclear collective deformed fluctuation

——— Without the influence

REFERENCES

[1] P. Grange, H. A. Weidenmuller, Phys. Lett. 96B, 26(1980)
P. Grange, Nucl. Phys. A428, 7(1984)
S. Hassani, P. Grange, Z. Phys. A325, 95(1986)
H. A. Weidenmuller, Nucl. Phys. A471, 1(1987)

[2] H. Delagrange et al., Z. Phys. A323, 497(1988)
C. Gregoire et al., Z. Phys. A329, 497(1988)

[3] H. S. Wio et al., Z. Phys. A334, 109(1989)

[4] David Brink, Nucl. Phys. A519 3C–16C(1990)

[5] Zhuo Yizhong et al., hsj–78239(lljs)

[6] S. Chandrasekhar, Rev. of Mod. Phys., 15, 1(1943)

[7] J. M. Sancho et al., J. Stat. Phys., 37, 151(1984)
M. Rodriguez et al., J. Stat. Phys., 40, 669(1988)

[8] Wang Shunuan, to be published in Il Nuovo Cimento

[9] N. Van Kanpen, " Stochastic Process in Phys. and Chemi." North Holland, Amsterdam (1983)

[10] Sun Ziyang et al., Z. Phys. A305, 61(1983)

[11] Su Zongdi et al., INDC(CPR)–2, (1986)

III DATA EVALUATION

THE EVALUATIONS AND THEORETICAL CALCULATIONS OF $^{235}U(p,n)^{235}Np$, $^{235}U(p,2n)^{234}Np$ AND $^{235}U(d,2n)^{235}Np$ REACTION CROSS SECTIONS

Zhuang Youxiang Shen Qingbiao

(CHINESE NUCLEAR DATA CENTER, IAE)

INTRODUCTION

The excitation functions of $^{235}U(p,n)^{235}Np$, $^{235}U(p,2n)^{234}Np$ and $^{235}U(d,2n)^{235}Np$ reactions were calculated and evaluated respectively.

Up to now, the experimental data for $^{235}U(p,n)$ and (p,2n) reactions in the energy region from threshold to 25 MeV have not been found; Argonne National Lab. (ANL)[1] and Lawrence Radiation Lab. at Berkeley (BRK)[2] have measured the excitation function of $^{235}U(d,2n)^{235}Np$ reaction respectively; but their data appear in great difference.

New experimental data have to wait for being measured for unpredictable time delays. In order to meet the practical requirements, the theoretical calculation and experimental evaluation are carried out.

1 THE THEORETICAL CALCULATIONS OF EXCITATION FUNCTIONS FOR $^{235}U(p,n)^{235}Np$ and $^{235}U(p,2n)^{234}Np$ REACTIONS

There is an only experimental measurement for $^{235}U(p,n)$ and (p,2n) reactions at BNL[3] of USA : $E_p = 200$ MeV, $\sigma_{p,n} = 0.48 \pm 0.05$ b, $\sigma_{p,2n} = 0.68 \pm 0.07$ mb. They are not quite enough for the base of theoretical calculation, because both existing data points are scarce, and the code CFUP1 is only suita-

ble for the energy region below 33 MeV now. However these data can be used as reference for model theory calculation.

The code CFUP1 based on the optical model and the unified treatment of excitation model and evaporation model can be used to calculate CPND of fissile nuclei.

According to Bohr postulation of that decay of compound nucleus is indeperelent of its formation, some statistical theory parameters obtained in calculations of neutron nuclear reactions on fissile nuclei are used in theoretical calculations of $p+^{235}U$; the universal parameters of some optical potentials are selected from those obtained by others. Therefore, the theoretical results (see table 1) are valuable more or less as reference values.

Table 1 The excitation functions of $^{235}U(p,n)^{235}Np$ and $^{235}U(p,2n)^{234}Np$ reactions calculated from code CFUP1

E_p (MeV)	5.0	6.0	6.5	7.0	8.0	9.0	10.0	11.0	12.0	13.0	14.0
$\sigma_{p,n}$ (mb)	0.001	0.027	0.097	0.249	0.538	1.038	2.276	4.205	6.094	7.511	8.536
$\sigma_{p,2n}$ (mb)					0.000	0.053	0.444	1.515	3.600	7.306	12.413

E_p (MeV)	14.5	15.0	16.0	17.0	18.0	19.0	20.0	21.0
$\sigma_{p,n}$ (mb)	8.936	9.283	9.859	10.328	10.697	10.914	10.903	10.635
$\sigma_{p,2n}$ (mb)	13.544	13.181	10.966	8.743	7.527	6.596	5.784	5.174

Comparing with the only experimental data at $E_p = 200$ MeV the trend of the theoretical calculation is reasonable, as shown in Fig. 1.

2 THE EVALUATION OF EXCITATION FUNCTION OF $^{235}U(d,2n)^{235}Np$ REACTION

The excitation function of $^{235}U(d,2n)^{235}Np$ reaction was measured by ANL[1] in 1959 and BRK[2] in 1966, respectively. Their results are listed in table 2.

Targets of ^{235}U of about 0.5 mg / cm^2 thickness were made by electroplating enriched ^{235}U (99.94 %) onto aluminium foils in ANL. The stacked foil technique of inserting weighed aluminium foils between target plates was used to obtain the desired bombarding energies, $E_d = 21.5 \sim 9.5$ MeV. The fluorescence yield of the L x-rays from ^{235}Np were counted in a scintillation spectrometer equipped with a 1 / 8-inch thick sodium iodide crystal and a

256–channel analyzer. It was necessary to subtract that of the L x–rays emitted by the spike ^{237}Np from the counting rates of the L x–rays of ^{235}Np. No any error analyses were given in this paper.

The electroplating enriched ^{235}U(>93%) targets and stacked foil technique are also used in BRK, E_d = 19.6~ 9.7 MeV. Counting rates of ^{235}Np were determined by resolution of decay curves obtained with the windowless proportional counter. Counting efficiency adopted was 70% for ^{235}Np. However, because of the uncertainties in the calibration of the instruments, systematic errors of 20% or more are possible in disintegration rates.

Random errors for the cross sections, derived from estimated uncertainties in target thickness, integrated beam current, chemical yield and counting rate, are approximately ± 20 %.

On the one hand, the fluorescence yields of L x–rays from ^{235}Np were measured at ANL only in a period of time, the fluorescence yield of ^{237}Np is difficult to be deduced; and the decay curves were measured at BRK in a long time (the half–lives are 396.2 days for ^{235}Np, 2.14×10^6 years for ^{237}Np). On the other hand, NaI crystal, which is usually enveloped in a dampproof cover, is difficult to be used to measure fluorescence yield; it is a better choice to measure the decay curves by windowless proportional counter. Thus the second method (BRK) is much better than the first one (ANL).

As shown in experimental results, no errors were given in the first method, it is possible that its measured accuracy was difficult to estimate, therefore, there is a big fluctuation in the result; the total errors of ± 28 % in cross sections were given in the second one. For the two reasons, the results of the latter are more accurate and reliable than the first, and adopted in this evaluation; the fitted values which are recommended for using are shown in table 3 and Fig. 2.

Table 2 The experimental data of $^{235}U(d,2n)^{235}Np$ reaction cross section

ANL, J. Wing et al.			BRK, R. M. Lessler et al.		
E_d (MeV)	σ (mb)	$\Delta\sigma$	E_d (MeV)	σ (mb)	$\Delta\sigma$ (%)
9.5	5.6		9.7	5.0	
11.4	16.3		10.9	13.0	
12.4	19.4		12.1	18.5	
13.4	26.7		14.2	13.8	28
14.8	24.4		15.2	13.0	
15.8	18.9		17.3	10.2	
16.7	18.3		19.3	8.72	
17.8	20.7				
18.6	18.0				
19.3	14.3				
20.0	16.2				
20.3	14.5				
21.5	19.6				

Table 3 The recommended values of $^{235}U(d,2n)^{235}Np$ reaction cross section

E_d (MeV)	9.7	10.0	10.5	11.0	11.5	12.0	12.5	13.0	13.5	14.0	14.5
$\sigma_{d,2n}$ (mb)	5.0	7.0	10.0	13.5	16.5	18.5	18.7	17.6	16.3	15.0	14.0
E_d (MeV)	15.0	15.5	16.0	16.5	17.0	17.5	18.0	18.5	19.0	19.5	20.0
$\sigma_{d,2n}$ (mb)	13.0	12.0	11.5	11.0	10.5	10.0	9.6	9.2	8.9	8.6	8.3

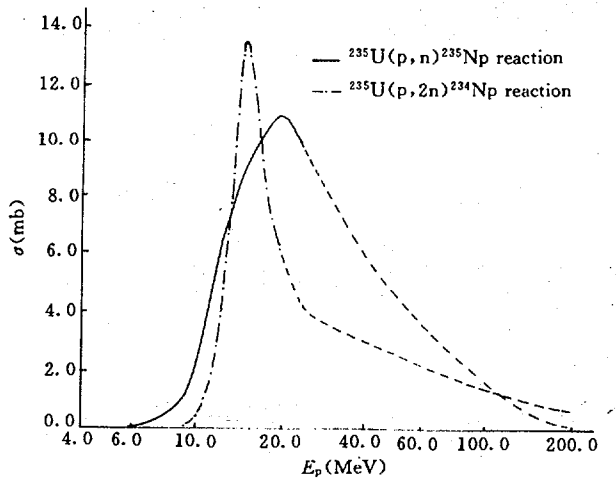

Fig. 1 Comparison of excitation functions of ^{235}U(p,n)^{235}Np and ^{235}U(p,2n)^{234}Np reactions calculated from CFUP1 with experimental data

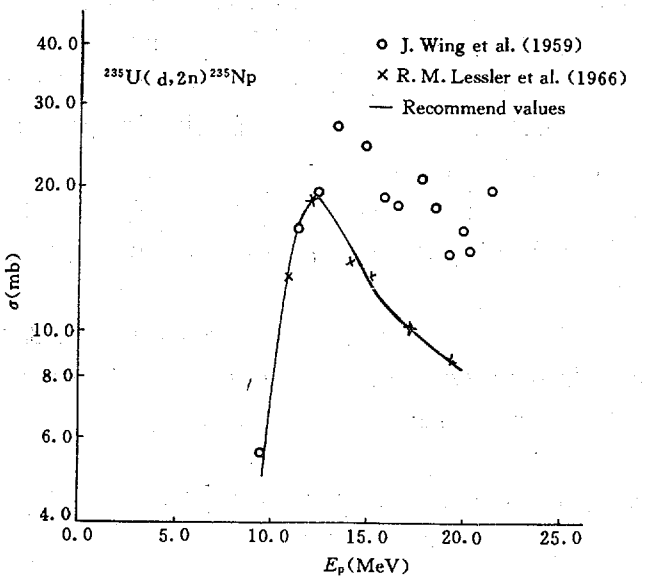

Fig. 2 The recommended values and experimental data of ^{235}U(d,2n)^{235}Np reaction cross section

REFERENCES

[1] J. Wing et al., PR, 114, 163(1959)

[2] R. M. Lessler et al., NP, 81, 401(1966)

[3] Y. Y. Chu et al., IRE, 30, 1153(1983)

IV ATOMIC AND MOLECULAR DATA

REFLECTION OF H AND D PLASMA PARTICLES FROM SOLID SURFACES

Yao Jinzhang Fang Shaohong Yu Hongwei

(CHINESE NUCLEAR DATA CENTER, IAE)

Data on particle and energy reflection coefficients of plasma particles at first wall materials in thermonuclear fusion devices are required for the assessment of the contribution of particle reflection in the particles recycling process and energy balance of plasma. Such data are available for many light ion–target combinations at normal and oblique incidence.

In the present work we have systematically analysed the oblique incident data by emperical formula for the combinations: H and D projectiles on B, Be, C, Al, Si Ti, Fe, Ni, Cu, Mo, W and Au elemental targets for incident energy range from 10 eV to 100 keV at incident angles of $0 < \theta < 75$ degrees.

Emperical formula is presented by R. Ito and T. Tabata et al.[1] (hereafter to be represented IT). The reflection coefficient R_n and R_e can be described as follows :

$$R_e = (0.705/f)/[1+(\varepsilon/0.047)^{0.597} + (\varepsilon/0.619)^{1.5}]$$

$f = F(\text{Energy}, Z_1, M_1, Z_2, M_2)$

ε = Reduced Energy

$$= 32.534\, M_2\, E_0/[Z_1\, Z_2\, (M_1 + M_2)\,(Z_1^{2/3} + Z_2^{2/3})^{1/2}]$$

E_0 = Incident Energy (keV)

Z_1, M_1 and Z_2, M_2 represent numbers of charge and mass for projectile and target respectively.

$$\gamma_e = 1/[1+(\varepsilon/0.133)^{0.285}] + 0.530/[1+(\varepsilon/85)^{-1.46}]$$

$$R_n = R_e/\gamma_e$$

For the dependence of the reflection coefficients on the angle of incidence. The following formula is given :

$$R(\theta) = R(0) + [1 - R(0)] / (1 + a_1 \cot^{2a_2} \theta)$$

$R(0)$ = Reflection coefficients for normal angle of incidence

$a_1 = 7.38 \quad a_2 = 0.836 / \varepsilon^{0.087}$ for R_n

$a_1 = 17.9 \quad a_2 = 0.771 / \varepsilon^{0.014}$ for R_e

RESULTS AND DISCUSSION

It has been presented that calculation results of reflection coefficients R_n and R_e of projectiles H and D on B, Be, C, Al, Si, Ti, Fe, Ni, Cu, Mo, W and Au targets by emperical formula (IT) within incident angles of 0 to 90 degrees. To comparing, the results calculated using PANDA-P (PP)[2] and some experimental values from different laboratories are also given. Figs. 1~4 show the results of R_n and R_e versus incident energy at normal incident angle of projectiles H and D on C, Fe and Au targets. The reflection coefficients are found to decrease with incident energy in the range of 10 eV to 100 keV. The relative deviations of the data from the emperical formula (IT) follow approximately the normal distribution; the standard deviation is 26 % for experimental data, and less than 30 % for calculated data by PP code. Figs. 5~8 represent the relations of R_n and R_e to incident energies for the combinations of H and D with carbon target. The dashed and solid curves indicated respectively calculations by IT and PP at incident angles of 0, 15, 30, 45, 60 and 75 degrees. The relations of R_n and R_e with angles of incidence are shown in Figs. 9~12 at the incident energy 10 eV, 100 eV, 1 keV, 10 keV, 100 keV for systems of H-C and D-C. Δ represents calculation of PP. The experimental values[3] are also shown in Fig. 11 at incident energy of 10 eV, 400 eV, 1 keV, 3 keV, 10 keV, 100 keV for combination of D with C.

For the low ratioes M_2 / M_1 (M_1 and M_2 mean mass of projectile and target), such as the combinations of H-C and D-C, the data are in well agreement within 100 eV to 10 keV incident energy range. For the high M_2 / M_1 ratioes, for instance, H-Fe and H-Au systems,the values from both calculations are in good agreement at incident energies of 1 keV to 100 keV.

REFERENCES

[1] R. Ito et al., IPPJ-AM-41

[2] Luo Zhengming et al., Nucl. Instr. Methods in Phys. Res. B48, 435(1990)

[3] C. K. Chen et al., Applied Phys. A33, 265(1984)

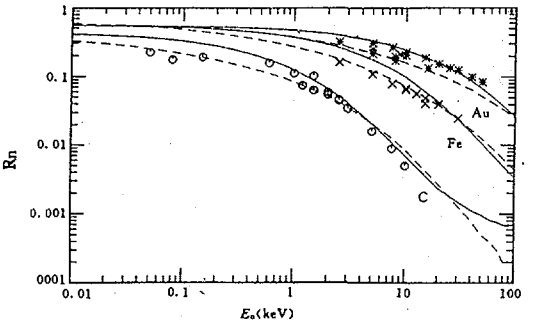

Fig. 1 R_n VS E_0 (keV) at normal incidence for H on C, Fe and Au

——— PP; – – – IT; ⊙ × * Represent Exp.

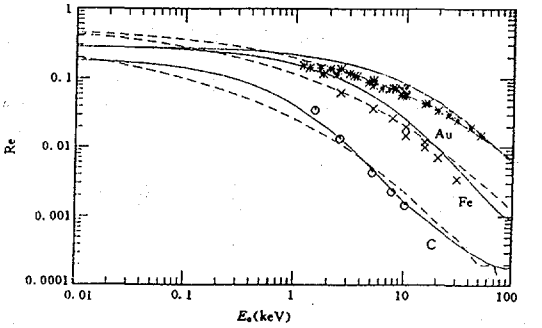

Fig. 2 The same as Fig. 1, except for R_e

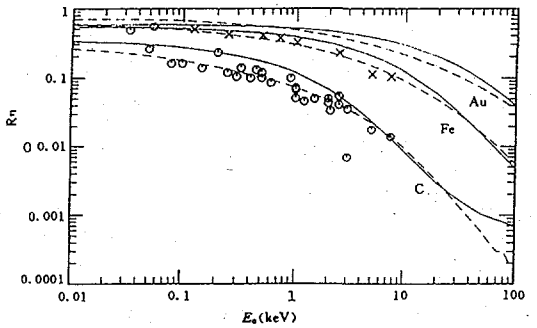

Fig. 3 R_n VS E_0 (keV) at normal incidence for D on C, Fe and Au

— PP; – – IT; ⊙ × Represent Exp.

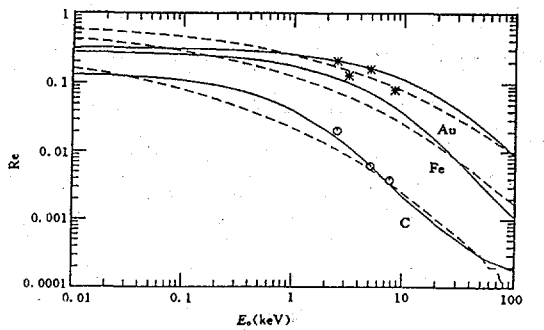

Fig. 4 The same as Fig. 3, except for R_e

— PP; – – IT; ⊙ * Represent Exp.

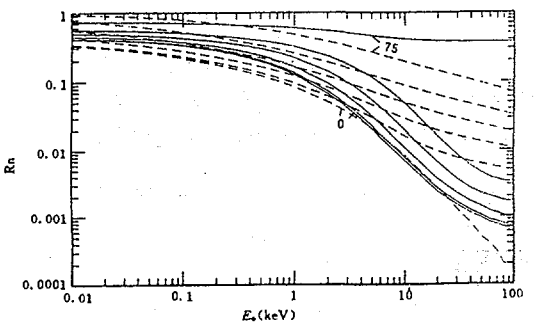

Fig. 5 R_n VS E_0 (keV) for H on C at inicdent angles 0, 15, 30, 45, 60 and 75 deg

——— PP; – – – IT.

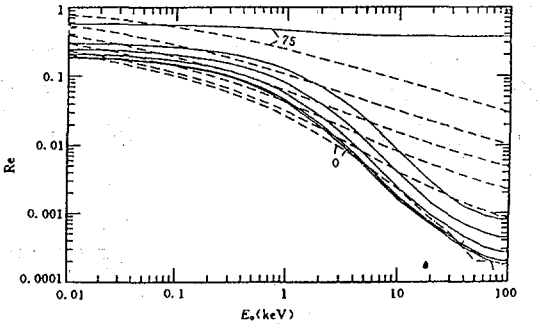

Fig. 6 The same as Fig. 5, except for R_e

——— PP; – – – IT.

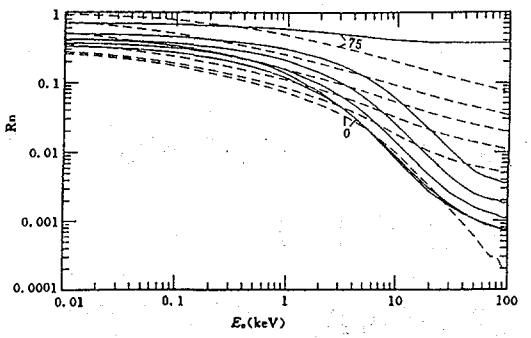

Fig. 7 R_n VS E_0 (keV) for D on C at inicdent angles 0, 15, 30, 45, 60 and 75 deg

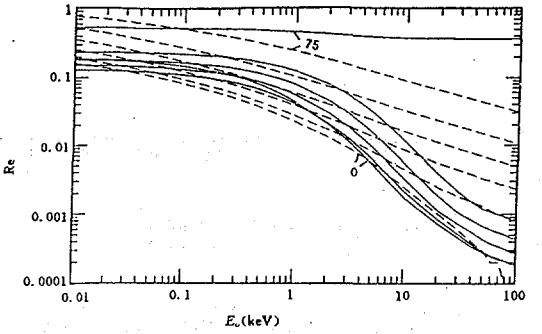

Fig. 8 The same as Fig. 7, except for R_e

——— PP; – – – IT.

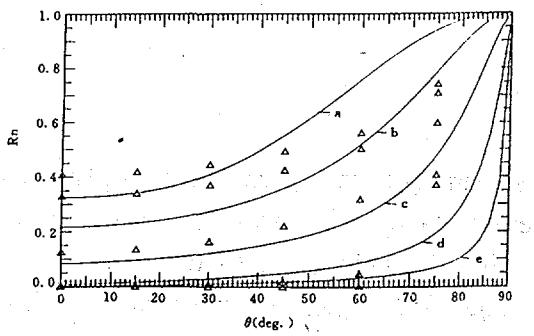

Fig. 9 R_n VS θ for H on C

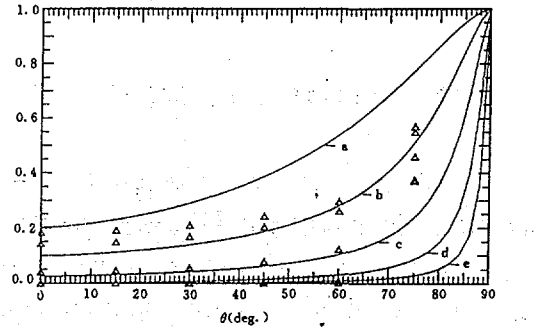

Fig. 10 R_e VS θ for H on C

——— IT; △–PP; E_0 = 0.01(a); 0.10(b); 1.0(c); 10(d) and 100(e) keV.

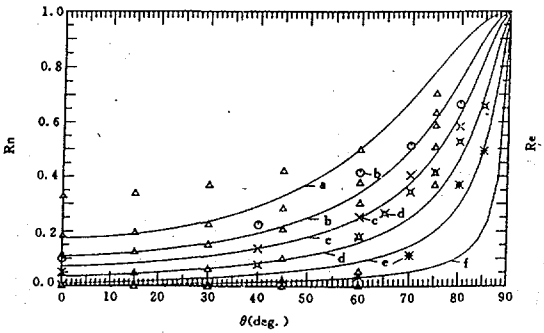

Fig. 11 R_n VS θ for D on C

——— IT; △–PP; E_0 = 0.01(a); 0.40(b); 1.0(c); 3.0(d), 10(e) and 100(f) keV.

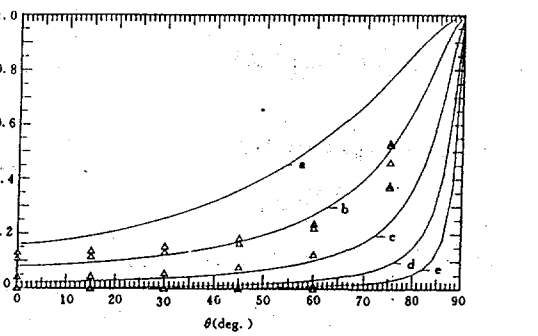

Fig. 12 R_e VS θ for D on C

——— IT; △–PP; E_0 = 0.01(a); 0.10(b); 1.0(c); 10(d); and 100(e) keV.

V DATA PROCESSING

METHOD AND CODE OF CURVE FITTING CONSIDERING THE UNCERTAINTIES ASSOCIATED WITH INDEPENDENT VARIABLES

Zhao Zhixiang

(CHINESE NUCLEAR DATA CENTER, IAE)

INTRODUCTION

The uncertaities associated with independent variables are usually neglected in curve fitting. Usually, the independent variables are also measured data, their uncertainties would affect the results of least square fitting and should be considered. For example, the incident energies of excitation function as independent variables are also measured data, their uncertainties are significant in the fitting of the derived quantities, especially for a rapidly varied function.

In this work, the formalism of least square fitting taking uncertainties associated with independent variables into account are derived and the code related was developed.

1 FORMALISM

Let us denote by

$$y = f(x;C) \tag{1}$$

the function to be fitted, where

$$C = (C_1 \cdots C_N)^t \tag{2}$$

are parameter vector to be adjusted fitting measured data X^* and Y^*

$$X^* = (x_1^* \cdots x_N^*)^t \tag{3}$$

$$Y^* = (y_1^* \cdots y_N^*)^t \tag{4}$$

To take the uncertainties of independent variables X^* into account in the fitting, we consider independent variables X also being the parameters to be fitted and require the results of the fitting satisfying the following constraint conditions

$$\hat{y}_i = f(\hat{x}_i; \hat{C}) \quad i = 1, \cdots, N \tag{5}$$

Let us define the vector of measured data

$$D^* = (X^* \quad y^*)^t \tag{6}$$

$$V_D = \begin{bmatrix} V_x & \mathrm{Cov}(X^*, Y^*) \\ \mathrm{Cov}(X^*, Y^*) & V_y \end{bmatrix} \tag{7}$$

The vector of measurement deviation is

$$\delta D = D^* - < D^* > \tag{8}$$

where

$$< D^* > = (X \quad Y)^t \tag{9}$$

$$X = (x_1 \cdots x_N)^t \tag{10}$$

$$Y = (y_1 \cdots y_N)^t \tag{11}$$

The objective function for least square fitting is

$$Q = \delta D^t V_D^{-1} \delta D \tag{12}$$

The parameters to be estimated are X and C, so $< D^* >$ must be expanded around kth iterated values, $X^{(k)}$ and $C^{(k)}$, it yields

$$\delta D \approx \delta D_k - T_k \delta P_k \tag{13}$$

where

$$\delta D_k = (X^* - X_0^{(k)} \quad Y^* - Y_0^{(k)})^t \tag{14}$$

$$X_0^{(k)}(i) = x_i^{(k)} \tag{15}$$

$$Y_0^{(k)}(i) = f_i^{(k)} = f(x_i^{(k)}; C^{(k)}) \tag{16}$$

$$\delta P_k = P - P^{(k)} \tag{17}$$

$$P = (X \quad C)^t \tag{18}$$

$$P^{(k)} = (X^{(k)} \quad C^{(k)})^t \tag{19}$$

$$T_k = \begin{bmatrix} I(N \times N) & O(N \times m) \\ F_x^{(k)}(N \times N) & F_c^{(k)}(N \times m) \end{bmatrix} \tag{20}$$

where I is a unit matrix and 0 a null matrix, and

$$F_x^{(k)}(i,i) = \frac{\partial f_i^{(k)}}{\partial x_i^{(k)}} \tag{21}$$

$$F_x^{(k)}(i,j) = 0 \qquad i \neq j \tag{22}$$

$$F_c^{(k)}(i,j) = \frac{\partial f_i^{(k)}}{\partial C_j^{(k)}} \tag{23}$$

Substituting Eq. (13) into Eq. (12) and minimizing Eq. (12) to P, we finally have

$$P^{(k+1)} = P^{(k)} + (T_k^t V_D^{-1} T_k)^{-1} T_k^t V_D^{-1} \delta D_k \tag{24}$$

$$V_p^{(k+1)} = (T_k^t V_D^{-1} T_k)^{-1} \tag{25}$$

Eqs. (24) and (25) represent the (k+1)–th iterated estimates for P and their covariance matrix.

2 CODE

Based on the formalism developed in Section 2, a code LSQXY, to deal with least square fitting with an arbitrary function $f(x;C)$ considering the uncertainties associated with independent variables X, has been developed.

In this code, the partial derivatives are calculated by the difference quotient. The form of $f(x;C)$, function to be fitted, can be written in a subroutine THEO by user. By re–writing THEO, user can readily deal with different physical problem. A general polynomial

$$f(x;C)=\sum_{j=1}^{m} C_j x^{j-1} \tag{25}$$

has been written in the code. The code LSQXY is available from the author.

3 EXAMPLE AND DISCUSSION

A computational example is given in Fig. 1. In this figure, the solid line represents the fitted curve taking the uncertaintites associated with independent variables X into account and the dotted line the fitted curve not considering the uncertainties of X. There is a significant difference between these two results.

ACKNOWLEDGEMENTS

The author would like to thank Drs. Zhou Delin, Chang Yongfu and Tu Jing for their helpful discussions.

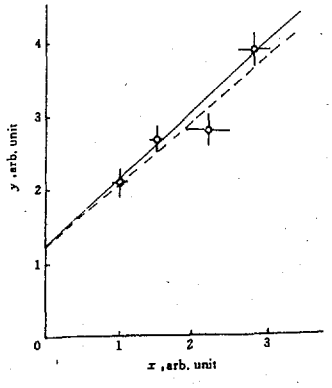

Fig. 1 An example of curve fitting considering the uncertainty of independent variable

CINDA INDEX

Nuclide	Quantity	Energy (eV)		Lab	Type	Documentation			
		Min	Max			Ref	Vol	Page	Date
^{9}Be	n Emission	1.47+6		SIU	Expt	Jour CNDP	8	3	Nov 92
^{40}Ca	(n,α)	4.0+6	5.0+6	BJG	Expt	Jour CNDP	8	7	Nov 92
^{54}V	Decay γ			NRS	Expt	Jour CNDP	8	16	Nov 92
^{56}Fe	Evaluation	5.0+6	5.0+7	AEP	Theo	Jour CNDP	8	20	Nov 92
^{56}Fe	Inelastic	1.4+7	2.0+7	AEP	Theo	Jour CNDP	8	35	Nov 92
^{89}Y	(p,x)	E_{th}	4.0+7	AEP	Theo	Jour CNDP	8	44	Nov 92
^{107}Ag	(α,n)	2.68+7		SIU	Expt	Jour CNDP	8	19	Nov 92
	(α,2n)	2.68+7		SIU	Expt	Jour CNDP	8	19	Nov 92
^{109}Ag	(α,2n)	2.68+7		SIU	Expt	Jour CNDP	8	19	Nov 92
^{235}U	(p,n)	5.0+6	2.1+7	AEP	Eval	Jour CNDP	8	65	Nov 92
	(p,2n)	9.0+6	2.1+7	AEP	Eval	Jour CNDP	8	65	Nov 92
	(d,2n)	9.7+6	2.0+7	AEP	Eval	Jour CNDP	8	65	Nov 92
^{238}U	Inelastic	1.4+7	2.0+7	AEP	Theo	Jour CNDP	8	35	Nov 92
	Inelastic	5.0+3	2.0+7	TSI	Theo	Jour CNDP	8	42	Nov 92
^{241}Am	(p,x)	5.5+6	3.5+7	AEP	Theo	Jour CNDP	8	52	Nov 92

Author, Comments
Zhang Kun+, TOF
Tang Guoyou+, Ion chamber, SIG, ANGDIS(T)
Chen Xueshi+, GE-LI, NAI
Shen Qingbiao+, CMUP2
Shen Qingbiao+, SIG, Coupled channel, DWBA
Shen Qingbiao+, SIG, CMUP2
Peng Xiufeng+, HPGe, ACTIV
Peng Xiufeng+, HPGe, ACTIV
Peng Xiufeng+, HPGe, ACTIV
Zhuang Youxiang+, SIG
Zhuang Youxiang+, SIG
Zhuang Youxiang+, SIG
Shen Qingbiao+, SIG, coupled channel, DWBA
Chen Zhenpeng, SIG, ECIS79
Shen Qingbiao+, CFUP1

核数据进展通讯(第8期)
原子能出版社出版
(北京2108信箱)
中国核数据中心排版
核科学技术情报研究所印刷
☆
开本 787×1092 1/16 · 印张 5 · 字数 80千字
1993年2月北京第一版 · 1993年2月北京第一次印刷
ISBN 7-5022-0864-X
TL · 557

COMMUNICATION OF NUCLEAR DATA PROGRESS

ISBN 7-5022-0864-X
TL · 55